Skeletal Muscle

RESEARCH

Open Access

Dysregulation of Tweak and Fn14 in skeletal muscle of spinal muscular atrophy mice

Katharina E. Meijboom[1,2], Emma R. Sutton[3], Eve McCallion[3], Emily McFall[4], Daniel Anthony[5], Benjamin Edwards[1], Sabrina Kubinski[6], Ines Tapken[6,7], Ines Bünermann[7], Gareth Hazell[1], Nina Ahlskog[1,8], Peter Claus[6,7], Kay E. Davies[1], Rashmi Kothary[4], Matthew J. A. Wood[1,8] and Melissa Bowerman[1,3,9*]

Abstract

Background: Spinal muscular atrophy (SMA) is a childhood neuromuscular disorder caused by depletion of the survival motor neuron (SMN) protein. SMA is characterized by the selective death of spinal cord motor neurons, leading to progressive muscle wasting. Loss of skeletal muscle in SMA is a combination of denervation-induced muscle atrophy and intrinsic muscle pathologies. Elucidation of the pathways involved is essential to identify the key molecules that contribute to and sustain muscle pathology. The tumor necrosis factor-like weak inducer of apoptosis (TWEAK)/TNF receptor superfamily member fibroblast growth factor-inducible 14 (Fn14) pathway has been shown to play a critical role in the regulation of denervation-induced muscle atrophy as well as muscle proliferation, differentiation, and metabolism in adults. However, it is not clear whether this pathway would be important in highly dynamic and developing muscle.

Methods: We thus investigated the potential role of the TWEAK/Fn14 pathway in SMA muscle pathology, using the severe Taiwanese *Smn*$^{-/-}$; *SMN2* and the less severe *Smn*$^{2B/-}$ SMA mice, which undergo a progressive neuromuscular decline in the first three post-natal weeks. We also used experimental models of denervation and muscle injury in pre-weaned wild-type (WT) animals and siRNA-mediated knockdown in C2C12 muscle cells to conduct additional mechanistic investigations.

Results: Here, we report significantly dysregulated expression of Tweak, Fn14, and previously proposed downstream effectors during disease progression in skeletal muscle of the two SMA mouse models. In addition, siRNA-mediated *Smn* knockdown in C2C12 myoblasts suggests a genetic interaction between Smn and the TWEAK/Fn14 pathway. Further analyses of SMA, *Tweak*$^{-/-}$, and *Fn14*$^{-/-}$ mice revealed dysregulated myopathy, myogenesis, and glucose metabolism pathways as a common skeletal muscle feature, providing further evidence in support of a relationship between the TWEAK/Fn14 pathway and Smn. Finally, administration of the TWEAK/Fn14 agonist Fc-TWEAK improved disease phenotypes in the two SMA mouse models.

Conclusions: Our study provides mechanistic insights into potential molecular players that contribute to muscle pathology in SMA and into likely differential responses of the TWEAK/Fn14 pathway in developing muscle.

Keywords: Spinal muscular atrophy, Survival motor neuron, Smn, Tweak, Fn14, Glucose metabolism, Skeletal muscle, Atrophy, Denervation

*Correspondence: m.bowerman@keele.ac.uk

[9] Wolfson Centre for Inherited Neuromuscular Disease, RJAH Orthopaedic Hospital, Oswestry, UK
Full list of author information is available at the end of the article

Background

The neuromuscular disease spinal muscular atrophy (SMA) is the leading genetic cause of infant mortality [1]. SMA is caused by mutations in the *survival motor*

neuron 1 (*SMN1*) gene [2]. The major pathological components of SMA pathogenesis are the selective loss of spinal cord alpha motor neurons and muscle wasting [3]. Skeletal muscle pathology is a clear contributor to SMA disease manifestation and progression and is caused by both denervation-induced muscle atrophy [4] and intrinsic defects [5, 6]. As skeletal muscle is the largest insulin-sensitive tissue in the body and is involved in glucose utilization [7], it is not surprising that muscle metabolism is also affected in SMA. Impaired metabolism has indeed been reported in SMA types 1, 2 and 3 patients [8]. A better understanding of the specific molecular effectors that contribute to SMA muscle physiopathology could provide mechanistic insights in SMA muscle pathology and help therapeutic endeavors aimed at improving muscle health in patients [9].

One pathway that plays a crucial role in chronic injury and muscle diseases is the tumor necrosis factor-like weak inducer of apoptosis (TWEAK) and its main signaling receptor, the TNF receptor superfamily member fibroblast growth factor-inducible 14 (Fn14) [10]. TWEAK is ubiquitously expressed and synthesized as a type 2 transmembrane protein but can also be cleaved by proteolytic processing and secreted as a soluble cytokine [10]. The role of the TWEAK/Fn14 pathway in skeletal muscle is conflicting as it has been demonstrated to have both beneficial and detrimental effects on muscle health and function [11, 12]. Indeed, pathologically high levels of TWEAK activate the canonical nuclear factor kappa-light-chain-enhancer of activated B cells (NF-κB) pathway, which promotes myoblast proliferation and thus inhibits myogenesis and the early phases of muscle repair and regeneration [13]. Conversely, lower physiological concentrations of TWEAK activate the non-canonical NF-κB pathway that promotes myoblast fusion and myogenesis [11]. The transmembrane protein Fn14 is typically dormant or present in low levels in normal healthy muscle [14]. Atrophic-inducing conditions (e.g. casting and surgical denervation) stimulate the expression of Fn14, leading to the chronic activation of the TWEAK/Fn14 pathway and sustained skeletal muscle atrophy [15]. We have also demonstrated an increased activity of the Tweak/Fn14 pathway in skeletal muscle of a mouse model of the neurodegenerative adult disorder amyotrophic lateral sclerosis (ALS), which is characterized by a progressive and chronic denervation-induced muscle atrophy [16]. In addition, various reported downstream effectors of the TWEAK/Fn14 pathway play critical roles in the regulation of muscle metabolism such as peroxisome proliferator-activated receptor-gamma coactivator 1α (PGC-1α), glucose transporter 4 (Glut-4), myogenic transcription factor 2d (Mef2d), hexokinase II (HKII) and Krüppel-like factor 15 (Klf15) [17–20].

Although the TWEAK/Fn14 pathway has been ascribed roles in both skeletal muscle health regulation and metabolism, both of which are impacted in SMA [9, 21], this pathway has yet to be investigated in the context of SMA. Furthermore, all research on this pathway has been performed in adult mice and therefore has never been explored in early phases of muscle development. We thus investigated the potential role of TWEAK and Fn14 in SMA and in early phases of post-natal skeletal muscle development. We report significantly decreased levels of both *Tweak* and *Fn14* during disease progression in two distinct SMA mouse models (*Smn*$^{-/-}$*;SMN2* and *Smn*$^{2B/-}$) [22, 23]. We also observed dysregulated expression of *PGC-1α*, *Glut-4*, *Mef2d* and *HKII*, previously proposed metabolic downstream effectors of TWEAK/Fn14 signaling [18, 24], in skeletal muscle of these SMA mice. In addition, more in-depth analyses revealed partial overlap of aberrantly expressed genes that regulate myopathy, myogenesis, and glucose metabolism pathways in skeletal muscle of SMA, *Tweak*$^{-/-}$ and *Fn14*$^{-/-}$ mice, further supporting potential shared functions between the TWEAK/Fn14 pathway and SMN in developing muscle. Finally, administration of Fc-TWEAK, an agonist of TWEAK/Fn14 signaling, improved disease phenotypes in the two SMA mouse models. Our study provides additional mechanistic insights into the potential molecular effectors that contribute to skeletal muscle pathology in SMA and suggests a role for the TWEAK/Fn14 pathway in the early stages of post-natal muscle development.

Methods

Animals and animal procedures

Wild-type mice FVB/N and C57BL/6J and the severe *Smn*$^{-/-}$*;SMN2* mouse model (FVB.Cg-Smn1tm1Hung Tg(SMN2)2Hung/J) [22] were obtained from the Jackson Laboratories. The *Smn*$^{2B/-}$ mouse model [23, 25] was kindly provided by Dr. Lyndsay M. Murray (University of Edinburgh). *Tweak*$^{-/-}$ [26] and *Fn14*$^{-/-}$ mouse models [27] were generously obtained from Linda C. Burkly (Biogen).

Smn$^{-/-}$*;SMN2* and *Smn*$^{+/-}$*;SMN2* mice were generated by breeding *Smn*$^{+/-}$ mice with *Smn*$^{-/-}$*;SMN2/SMN2* mice as previously described [28]. *Smn*$^{2B/-}$ and *Smn*$^{2B/+}$ mice were generated by breeding *Smn*$^{2B/2B}$ and *Smn*$^{+/-}$ mice as previously described [23].

Experimental procedures with live animals were authorized and approved by the University of Oxford ethics committee and UK Home Office (current project license PDFEDC6F0, previous project license 30/2907) in accordance with the Animals (Scientific Procedures) Act 1986, the Keele University Animal Welfare Ethical Review Body and UK Home Office (Project License P99AB3B95) in accordance with the Animals (Scientific

Procedures) Act 1986, the University of Ottawa Animal Care Committee according to procedures authorized by the Canadian Council on Animal Care and the German Animal Welfare law, and approved by the Lower Saxony State Office for Consumer Protection and Food Safety (LAVES, reference numbers 15/1774 and 19/3309).

Fc-TWEAK was administered by subcutaneous injections using a sterile 0.1 cc insulin syringe at various doses (7.9 μg, 15.8 μg, or 31.6 μg) and at a volume of 20 μl either daily, every other day, or every 4 days. Mouse Fc-TWEAK, a fusion protein with the murine IgG2a Fc region, and Ig isotope control were kindly provided by Linda C. Burkly (Biogen) [26].

For survival studies, mice were weighed and monitored daily and culled upon reaching their defined humane endpoint.

For all experiments, litters were randomly assigned at birth, and whole litters composed of both sexes were used. Sample sizes were determined based on similar studies with SMA mice.

To reduce the total number of mice used, the fast-twitch *tibialis anterior* (TA) and triceps muscles from the same mice were used interchangeably for respective molecular and histological analyses.

Sciatic nerve crush and cut

For nerve crush and cut experiments, post-natal day (P) 7 wild-type (WT) FVB/N mice were anesthetized with 2% isoflurane/oxygen before one of their lateral thighs was shaved and a 1 cm incision in the skin was made over the lateral femur. The muscle layers were split with blunt scissors and the sciatic nerve localized and crushed with tweezers for 15 s for the nerve crush. For the nerve cut, an ~2-mm section of the nerve was removed and the transection was confirmed under an operating microscope at ×12.8. The skin incision was closed with surgical glue, and animals were allowed to recover on a warming blanket. Ipsilateral and contralateral TA muscles were harvested at P14 and either fixed in 4% paraformaldehyde (PFA) for 24 h for histological analyses or snap frozen for molecular analyses.

Cardiotoxin injections

Cardiotoxin γ (Cytotoxin I, Latoxan, L8102, Portes les Valence) was dissolved in 0.9% saline and injected 4 μl/g per total mouse weight of a 10 μM solution into the left TA muscle of WT FVB/N mice at P10. The right TA was injected with equal volumes of 0.9% saline. During the injection, mice were anesthetized with 2% isoflurane/oxygen, and all injections were done using a sterile 0.3 cc insulin syringe. TA muscles were harvested 6 days later and either fixed in 4% PFA for 24 h for histological analyses or snap frozen for molecular analyses.

Laminin staining of skeletal muscle

TA muscles were fixed in PFA overnight. Tissues were sectioned (13 μm) and incubated in blocking buffer for 2 h (0.3% Triton-X, 20% fetal bovine serum (FBS) and 20% normal goat serum in PBS). After blocking, tissues were stained overnight at 4 °C with rat anti-laminin (1:1000, Sigma L0663) in blocking buffer. The next day, tissues were washed in PBS and probed using a goat-anti-rat IgG 488 secondary antibody (1:500, Invitrogen A-11006) for 1 h. PBS-washed tissues were mounted in Fluoromount-G (Southern Biotech). Images were taken with a DM IRB microscope (Leica) with a 20× objective. Quantitative assays were performed blinded on 3–5 mice for each group and five sections per mouse. The area of muscle fiber within designated regions of the TA muscle sections was measured using Fiji (ImageJ) [29].

Hematoxylin and eosin staining of skeletal muscle

TA muscles were fixated in 4% PFA and imbedded into paraffin blocks. For staining, muscles were sectioned (13 μm) and deparaffinized in xylene and then fixed in 100% ethanol. Following a rinse in water, samples were stained in hematoxylin (Fisher) for 3 min, rinsed in water, dipped 40 times in a solution of 0.02% HCl in 70% ethanol, and rinsed in water again. The sections were next stained in a 1% eosin solution (BDH) for 1 min, dehydrated in ethanol, cleared in xylene, and mounted with Fluoromount-G (Southern Biotech).

Images were taken with a DM IRB microscope (Leica) with a 20× objective. Quantitative assays were performed blinded on 3–5 mice for each group and five sections per mouse. The area of muscle fiber within designated regions of the TA muscle sections was measured using Fiji (ImageJ) [29].

Cell culture

Both C2C12 myoblasts [30] and NSC-34 neuronal-like cells [31] were maintained in growth media consisting of Dulbecco's Modified Eagle's Media (DMEM) supplemented with 10% FBS and 1% penicillin/streptomycin (all Life Technologies). Cells were cultured at 37 °C with 5% CO_2. C2C12 myoblasts were differentiated in DMEM containing 2% horse serum for 7 days to form multinucleated myotubes. Cells were regularly tested for mycoplasma and remained mycoplasma-free.

In vitro siRNA knockdown

For small interfering RNA (siRNA) transfections, C2C12 myoblasts were seeded onto 12-well plates at a 50% confluency and cultured overnight in 2 mL of DMEM. Cells were washed with PBS prior to siRNA transfection, whereby 100 pmol of each siRNA (*Tweak*, *Fn14*,

Smn) (Invitrogen, assay IDs s233937, s203164, s74017, respectively) in a complex with 10 µl of Lipofectamine RNAi/MAX (Invitrogen) dissolved in OptiMEM solution (Gibco) was added to the cells for 3 h. The transfection mix was then substituted either for DMEM without the siRNAs for 1 day or with a differentiation medium mix without the siRNAs for 7 days.

qPCR

RNA was extracted from tissues and cells either by a RNeasy kit from Qiagen or by a Isolate II RNA Mini Kit from Bioline or by guanidinium thiocyantate-acid-phenol-chloroform extraction using TRIzol Reagent (Life Technologies) as per manufacturer's instructions. The same RNA extraction method was employed for similar experiments and equal RNA amounts were used between samples within the same experiments. cDNA was prepared with the High-Capacity cDNA Kit (Life Technologies) or qPCRBIO cDNA Synthesis Kit (PBCR Biosystems) according to the manufacturer's instructions. The same reverse transcription method was employed for similar experiments. The cDNA template was amplified on a StepOnePlus Real-Time PCR Thermocycler (Life Technologies) with SYBR Green Mastermix from Applied Biosystems or with qPCRBIO SyGreen Blue Mix Hi-ROX (PCR Biosystems). The same amplification method was used for similar experiments. qPCR data was analyzed using the StepOne Software v2.3 (Applied Biosystems). Primers used for qPCR were obtained from IDT and sequences for primers were either self-designed or ready-made (Supplementary Table 1). Relative gene expression was quantified using the Pfaffl method [32], and primer efficiencies were calculated with the LinReg-PCR software. We normalized relative expression level of all tested genes in mouse tissue and cells to *RNA polymerase II polypeptide J* (*PolJ*) [33]. For all qPCR graphs, the normalized expression of the experimental groups is compared to a referent group, for which the normalized expression values were set to 1 by multiplying the normalized expression of each referent sample in that group by the value corresponding to 1/(average of all samples in that referent experimental group). That value was then used to multiply the normalized relative expression of each sample in all experimental groups.

PCR array

RNA was extracted using the RNeasy® Microarray Tissue Kit (Qiagen). cDNA was generated with the RT^2 First Strand Kit (Qiagen). qPCRs were performed using RT^2 Profiler™ PCR Array Mouse Skeletal Muscle: Myogenesis and Myopathy Mouse (PAMM-099Z, SABiosciences) and RT^2 Profiler™ PCR Array Mouse Glucose Metabolism (PAMM-006Z SABiosciences). The data were analyzed with RT Profiler PCR Array Data Analysis (version 3.5), and mRNA expression was normalized to the two most stably expressed genes between all samples. We used the publicly available database STRING (version 11.5) for network and enrichment analysis of differently expressed genes [34]. The minimum required interaction score was set at 0.4, medium confidence.

Western blot

For westerns in Fig. 1, freshly prepared radioimmunoprecipitation (RIPA) buffer was used to homogenize tissue and cells, consisting of 50 mM Tris pH 8.8, 150 mM NaCl, 1% NP-40, 0.5% sodium deoxycholate, 0.1% SDS, and complete mini-proteinase inhibitors (Roche). Equal amounts of total protein were loaded, as measured by Bradford assay. Protein samples were first diluted 1:1 with Laemmli sample buffer (Bio-Rad, Hemel Hempstead, UK) containing 5% β-mercaptoethanol (Sigma) and heated at 100 °C for 10 min. Next, samples were loaded on freshly made 1.5 mm 12% polyacrylamide separating and 5% stacking gel, and electrophoresis was performed at 120 V for ~1.5 h in running buffer. Subsequently, proteins were transferred from the gel onto to a polyvinylidene fluoride membrane (Merck Millipore) via electroblotting at 120 V for 60 min in transfer buffer containing 20% methanol. Membranes were then incubated for 2 h in Odyssey Blocking Buffer (Licor). The membrane was then probed overnight at 4 °C with primary antibodies (P105/p50, 1:1000, Abcam ab32360; Actin, 1:1000, Abcam ab3280) in Odyssey Blocking Buffer and 0.1% Tween-20. The next day, after three 10-min washing

(See figure on next page.)

Fig. 1 Aberrant expression of Tweak and Fn14 in skeletal muscle of *Smn*$^{-/-}$*;SMN2* SMA mice. **a**–**g** qPCR analysis of *parvalbumin* (**a**), *Tweak* (**b**), *Fn14* (**c**), *Pgc-1α* (**d**), *Mef2d* (**e**), *Glut-4* (**f**), and *HKII* (**g**) in triceps, gastrocnemius, TA, and quadriceps muscles from postnatal day (P) 0 (birth), P2 (pre-symptomatic), P5 (early symptomatic), P7 (late symptomatic), and P19 (end stage) *Smn*$^{-/-}$*;SMN2* and wild-type (WT) mice. Normalized relative expressions are compared to WT P0. Data are mean ± SEM, $n = 3$-4 animals per experimental group, two-way ANOVA, Sidak's multiple comparison test between genotypes, *$p < 0.05$, **$p < 0.01$, ***$p < 0.001$, ****$p < 0.0001$. **h**–**i** Quantification of NF-κB p50/actin protein levels in the TA of pre-symptomatic (P2) (**h**) and late-symptomatic (P7) (**i**) *Smn*$^{-/-}$*;SMN2* mice and age-matched WT animals. Images are representative immunoblots. Data are mean ± SEM, $n = 3$–4 animals per experimental group, unpaired *t*-test, ns, not significant (**h**), $p = 0.0215$ (**i**). **j** Quantification of NF-κB p50/actin and p105/actin protein levels in the quadriceps (quad) of late-symptomatic (P7) *Smn*$^{-/-}$*;SMN2* mice and age-matched WT animals. Images are representative immunoblots. Data are mean ± SEM, $n = 3$–4 animals per experimental group, two-way ANOVA, uncorrected Fisher's LSD, ****$p < 0.0001$, ns, not significant. **k** qPCR analysis *NF-κB-inducing kinase* (*NIK*) in TA muscle of late-symptomatic P7 *Smn*$^{-/-}$*;SMN2* and age-matched WT animals. Data are mean ± SEM, $n = 3$–4 animals per experimental group, unpaired *t*-test, $p = 0.0094$

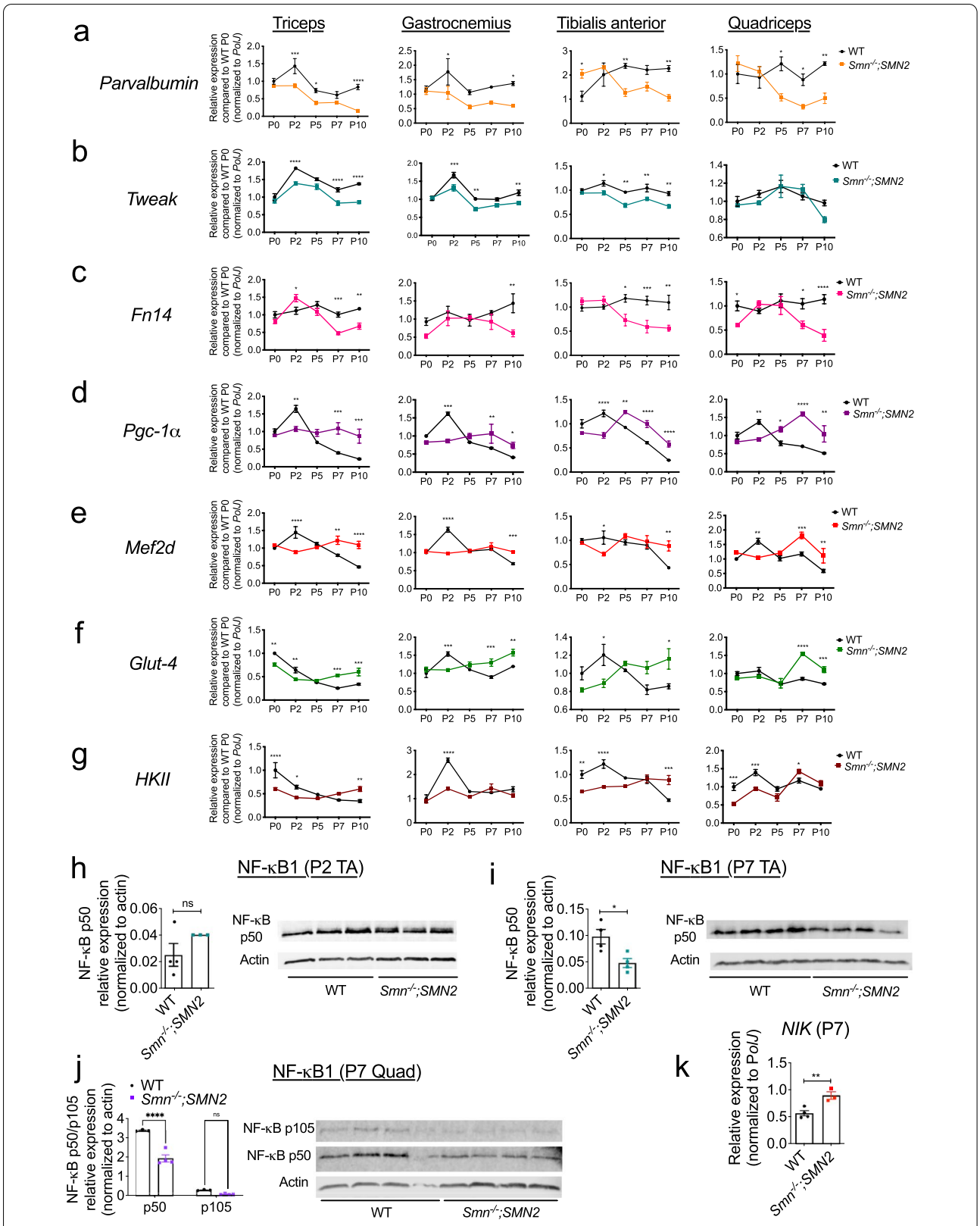

Fig. 1 (See legend on previous page.)

steps with PBS, the membrane was incubated for 1 h at room temperature with secondary antibodies (goat anti-rabbit IgG 680RD, 1:1000, LI-COR 926-68071; goat anti-mouse IgG 800CW, 1:1000 LI-COR, 926-32210). Lastly, the membrane was washed three times for 10 min in PBS and visualized by scanning 700 nm and 800 nm channels on the LI-COR Odyssey CLx infrared imaging system (LI-COR) for 2.5 min per channel. The background was subtracted, and signal of protein of interest was divided by signal of the housekeeping protein.

For westerns in all others figures, the same steps were followed with the following key differences. Bio-Rad TGX Stain-Free gels were used, and gels were imaged on a ChemiDoc Bio-Rad Imager before transfer to quantify total protein used for normalization. The primary antibodies used were NF-κB2 p100/p52 (Cell Signaling, no. 4882, 1:1000), NF-κB1 p105/p50 (Cell Signaling, no. 12540, 1:1000), and Tweak (Abcam, ab37170, 1:1000). The secondary antibody used was goat anti-rabbit IgG secondary Dylight 800 (Invitrogen, SA5-100036, 1:10000). Quantification was performed using the Bio-Rad Image Lab software.

Statistical analysis

All statistical analyses were done with the most up to date GraphPad Prism software. When appropriate, a Student's unpaired two-tail *t*-test, a one-way ANOVA, or a two-way ANOVA was used. Post hoc analyses used are specified in figure legends. Outliers were identified via the Grubbs' test. For the Kaplan-Meier survival analysis, the log-rank test was used and survival curves were considered significantly different at $p < 0.05$.

Results

Tweak and Fn14 are dysregulated in two SMA mouse models

We firstly investigated the expression of Tweak and Fn14 in skeletal muscle of the severe Taiwanese *Smn*$^{-/-}$*;SMN2* mouse model [22], using muscles with reported differential vulnerability to neuromuscular junction (NMJ) denervation (vulnerability: triceps brachii > gastrocnemius > TA > quadriceps femoris) [35]. Muscles were harvested from *Smn*$^{-/-}$*;SMN2* and WT mice at several time points during disease progression: birth (post-natal day (P) 0, pre-symptomatic (P2), early symptomatic (P5), late symptomatic (P7), and end stage (P10)). Muscle pathology in this SMA mouse model during disease progression has been well documented [36, 37].

We assessed the expression of *parvalbumin*, a high affinity Ca^{2+}-binding protein, which is downregulated in denervated muscle [38, 39] and a marker of muscle atrophy in skeletal muscle of SMA patients and *Smn*$^{-/-}$*;SMN2* mice [40]. We observed a significant decreased expression of *parvalbumin* mRNA during disease progression (Fig. 1a) in SMA mice compared to WT animals, further confirming parvalbumin as a *bona fide* marker of muscle atrophy in SMA [40]. Furthermore, we noted that *parvalbumin* expression was downregulated at earlier time points in the two most vulnerable muscles (triceps and gastrocnemius) [35] of SMA mice compared to WT animals (Fig. 1a).

We next evaluated the expression of *Tweak* and *Fn14* and observed significant decreased levels of *Tweak* mRNA in muscles of *Smn*$^{-/-}$*;SMN2* mice during disease progression, except in the quadriceps (Fig. 1b). Similarly, we found significantly lower levels of *Fn14* mRNA in all muscles of *Smn*$^{-/-}$*;SMN2* mice during disease progression (Fig. 1c) compared to WT animals. Interestingly, the decreased expression of *Fn14* in denervated and atrophied muscles of neonatal animals is different to previous reports in adults where denervation-induced atrophy stimulates its expression [15, 16].

As mentioned above, the TWEAK/Fn14 pathway has been reported to negatively influence the expression of metabolic effectors Klf15, Pgc-1α, Mef2d, Glut-4 and HKII [18]. Given that we have previously published a concordant increased expression of *Klf15* in skeletal muscle of SMA mice during disease progression [41], we next evaluated if the additional metabolic targets proposed to be modulated by Tweak and Fn14 were similarly dysregulated in the predicted directions. We indeed observed that the mRNA expression of *Pgc-1α*, *Mef2d*, *Glut-4* and *HKII* was significantly upregulated in muscles of *Smn*$^{-/-}$*;SMN2* mice at symptomatic time points (P5–P10) compared to WT animals (Fig. 1d–g), showing an expected opposite pattern to both *Tweak* and *Fn14* (Fig. 1b–c) [18]. Notably, we also found that in most muscles, mRNA levels of *Pgc-1α*, *Mef2d*, *Glut4* and *HKII* were significantly decreased in pre-symptomatic *Smn*$^{-/-}$*;SMN2* mice (P0–P5) compared to WT animals (Fig. 1d–g), independently of *Tweak* and *Fn14* (Fig. 1b–c).

TWEAK and Fn14 have also been reported to impact the canonical and non-canonical NF-κB pathways in skeletal muscle [42, 43]. In pre-symptomatic (P2) TA muscle, we observed no significant difference in the expression of NF-κB1 (p50), a component of the canonical NF-κB pathway, between *Smn*$^{-/-}$*;SMN2* mice and WT animals (Fig. 1h), consistent with normal *Tweak* and *Fn14* levels (Fig. 1b–c). Conversely, there was a significant decreased expression of NF-κB1 (p50) in TA muscle of symptomatic *Smn*$^{-/-}$*;SMN2* mice compared to WT animals at P7 (Fig. 1i), in line with reduced levels of *Tweak* and *Fn14* (Fig. 1b). These findings are validated in P7 quadriceps, where NF-κB1 (p50) levels are also significantly decreased in *Smn*$^{-/-}$*;SMN2* mice compared to WT animals (Fig. 1j). We found no significant

difference for the p105 NF-κB1 component. Of note, for all NF-κB1 p50/105 westerns, the p105 component was always more difficult to detect and sometimes even undetectable such as was the case for P7 TAs. We also investigated the expression of NF-κB-inducing kinase (NIK), involved in the non-canonical NF-κB activation pathway [44]. We observed that mRNA levels of *NIK* were significantly increased in TA muscle of P7 $Smn^{-/-}$;*SMN2* mice compared to WT animals (Fig. 1k), suggesting that dysregulated activity of Tweak and Fn14 in skeletal muscle of SMA mice may influence both the canonical and non-canonical NF-κB pathways, which play key regulatory roles in muscle health and metabolism [11, 12].

Finally, we evaluated the expression of Tweak and Fn14 in skeletal muscle of the less severe $Smn^{2B/-}$ mouse model of SMA [23]. TA muscles were harvested from $Smn^{2B/-}$ mice and age-matched WT animals at P0 (birth), P2 (early pre-symptomatic), P4 (late pre-symptomatic), P11 (early symptomatic), and P19 (end stage). Similar to the $Smn^{-/-}$;*SMN2* mice, muscle pathology in this SMA mouse model during disease progression has been well documented [36, 37]. We found a significant decreased expression of *parvalbumin* (Fig. 2a), *Tweak* (Fig. 2b) and *Fn14* (Fig. 2c) in muscle from $Smn^{2B/-}$ mice during disease progression compared to WT animals, similar to that observed in the more severe $Smn^{-/-}$;*SMN2* SMA mouse model (Fig. 1a–c). We have previously reported the aberrant increased expression of *Klf15* in the TA muscle of $Smn^{2B/-}$ mice during disease progression [41]. However, *Pgc-1α* expression was increased at P11 only (Fig. 2d), *Mef2d* at P2 only (Fig. 2e), *Glut-4* at P11 only (Fig. 2f), while *HKII* was significantly decreased at P0 and P19 and significantly increased at P4 (Fig. 2g), suggesting that the proposed negative impact of Tweak and Fn14 activity on these metabolic effectors may be dependent on disease severity, age, and/or genetic strain. Tweak downregulation in triceps of P18 $Smn^{2B/-}$ mice was confirmed by western (Fig. 2h). Furthermore, contrary to what was observed in the $Smn^{-/-}$;*SMN2* mice, there was no significant difference in the NF-κB1 p50 component but a significant decreased expression of the NF-κB1 p105 component in skeletal muscle of $Smn^{2B/-}$ mice compared to WT animals (Fig. 2i). For the NF-κB2 pathway, we found no significant difference for either the p52 or the p100 components (Fig. 2j). Thus, our results point to distinct profiles of the NF-κB1 and 2 pathways in skeletal muscle of the two SMA mouse models, which could be due to differential expression and/or processing of the components and to non-Tweak/Fn14 pathways.

To determine if the dysregulated expression of Tweak, Fn14, and the previously reported metabolic effectors in SMA muscle is independent of disease status, we investigated the mRNA expression of *Tweak*, *Fn14*, *Pgc-1α*, *Mef2d*, *Glut-4*, *HKII* and *Klf15* in triceps of P7 WT, $Smn^{2B/2B}$ and $Smn^{+/-}$ mice (Supplementary Fig. 1), a time point at which significant changes were already observed in the $Smn^{-/-}$;*SMN2* mice. $Smn^{2B/2B}$ and $Smn^{+/-}$ mice express ~70% and 50% of full-length functional Smn protein compared to WT animals, respectively, and do not display a canonical SMA phenotype [23, 45]. While we found some instances of differential expression (*Glut-4*: $Smn^{2B/2B}$ vs $Smn^{+/-}$, *HKII*: $Smn^{2B/2B}$ vs $Smn^{+/-}$ and *Klf15*: WT vs $Smn^{+/-}$), there is no clear correlation between non-pathological Smn levels (WT vs $Smn^{2B/2B}$ vs $Smn^{+/-}$) and expression of molecular components associated with the Tweak/Fn14 pathway (Supplementary Fig. 1).

We have thus demonstrated that Tweak, Fn14, and associated metabolic effectors are dysregulated during progressive muscle atrophy in two SMA mouse models, and that this is most likely due to pathological levels of Smn depletion.

Denervation does not affect Tweak and Fn14 during the early stages of muscle development

As SMA muscle pathology is defined by both intrinsic defects and denervation-induced events, we set out to determine which of these may influence the dysregulation of Tweak and Fn14 in SMA muscle. We firstly addressed the denervation component by performing nerve crush experiments in which the sciatic nerves of P7 WT mice were crushed and the muscle harvested at P14 [46]. Of note, the sciatic nerve was crushed in only one hind limb, leaving the other control hindlimb intact. Quantification of myofiber area in TA muscles showed a

(See figure on next page.)

Fig. 2 Aberrant expression of Tweak and Fn14 in skeletal muscle of $Smn^{2B/-}$SMA mice. **a**–**g** qPCR analysis of *parvalbumin* (**a**), *Tweak* (**b**), *Fn14* (**c**), *Pgc-1α* (**d**), *Mef2d* (**e**), *Glut-4* (**f**), and *HKII* (**g**) in TA muscles from P0 (birth), P2 (pre-symptomatic), P4 (pre-symptomatic), P11 (early symptomatic), and P19 (end stage) $Smn^{2B/-}$ and WT mice. Normalized relative expressions are compared to WT P0. Data are mean ± SEM, $n = 3$–4 animals per experimental group, two-way ANOVA, Sidak's multiple comparison test between genotypes, *$p < 0.05$, **$p < 0.01$, ***$p < 0.001$, ****$p < 0.0001$. **h** Quantification of Tweak protein levels normalized to total protein in the triceps of late-symptomatic (P18) $Smn^{2B/-}$ mice and age-matched WT animals. Images are representative immunoblots. Data are mean ± SEM, $n = 6$–7 animals per experimental group, unpaired *t*-test, $p = 0.014$. **i** Quantification of NF-κB1 p50 and p105 protein levels normalized to total protein in the triceps of late-symptomatic (P18) $Smn^{2B/-}$ mice and age-matched WT animals. Images are representative immunoblots. Data are mean ± SEM, $n = 6$–7 animals per experimental group, unpaired *t*-test, *ns*, not significant (p50), $p = 0.0354$ (p105). **j** Quantification of NF-κB2 p52 and p100 protein levels normalized to total protein in the triceps of late-symptomatic (P18) $Smn^{2B/-}$ mice and age-matched WT animals. Images are representative immunoblots. Data are mean ± SEM, $n = 3$–4 animals per experimental group, unpaired *t* test, ns, not significant (p52), $p = 0.0532$ (p100)

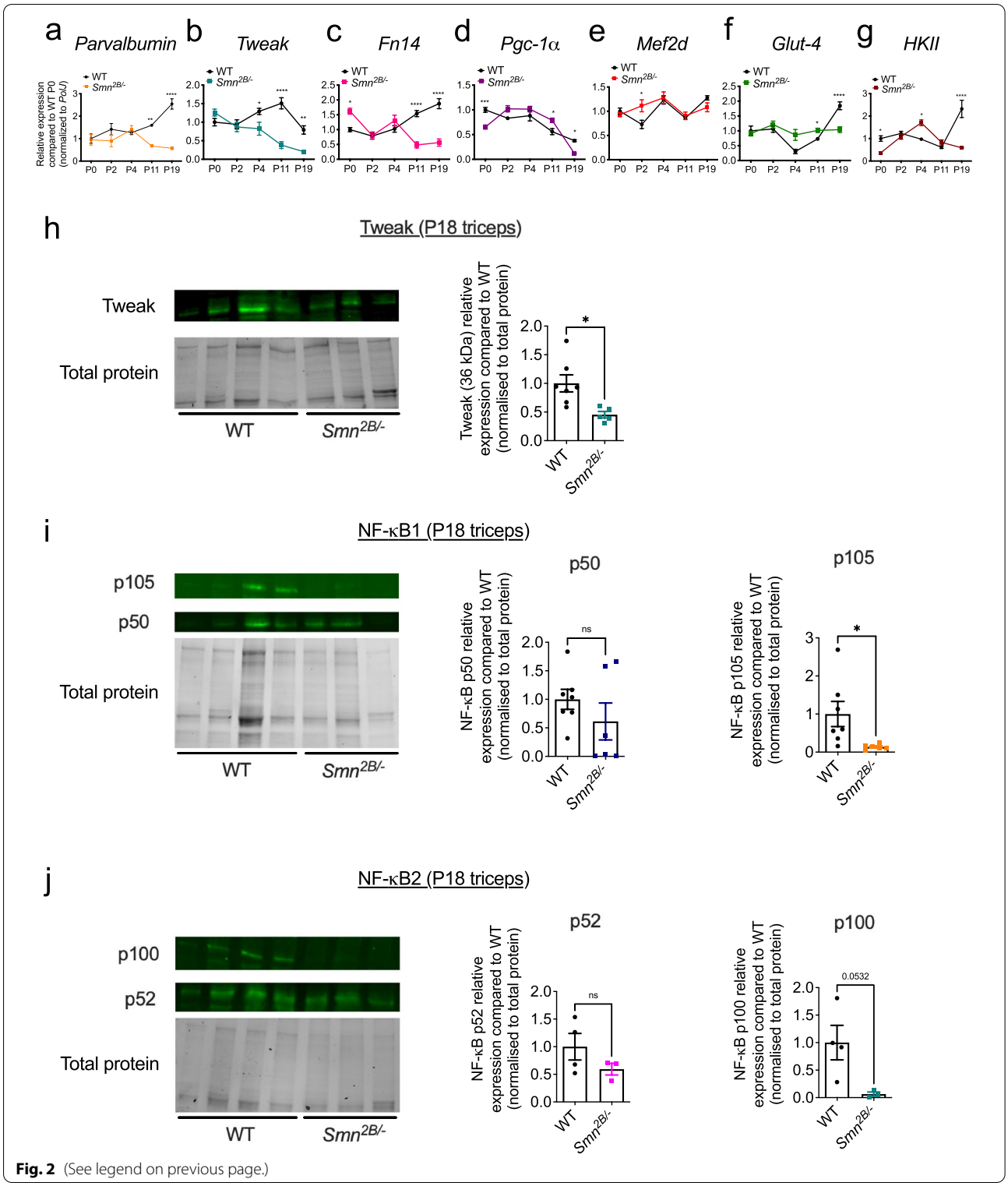

Fig. 2 (See legend on previous page.)

significant decrease in myofiber size in the nerve crush muscle compared to the control hind limb (Fig. 3a–c).

Expression analyses further revealed that there were no significant changes in mRNA levels of *parvalbumin*, *Tweak*, *Fn14*, *PGC-1α*, *Mefd2*, *Glut-4* and *HKII* in the denervated muscle compared to the control TA muscle (Fig. 3d). Interestingly, while denervation in adult muscle has previously been reported to induce a dramatic

surge in Fn14 expression [15, 16], this did not occur in the denervated muscles of our pre-weaned mice, suggesting an age and/or development regulatory element to this response. We also investigated the expression of *Klf15* and *Smn* and similarly observed no significant differences between the nerve crush and control muscles (Fig. 3d). To ensure that our results were not influenced by the potential reinnervation of muscles following a nerve crush, we repeated the experiments by performing a nerve cut instead. We observed that this complete denervation of TAs in pre-weaned mice does not significantly impact the mRNA expression of *Tweak*, *Fn14*, *PGC-1α*, *Mefd2*, *Glut-4*, *HKII* and *Klf15* compared to uninjured control hind limbs (Supplementary Fig. 2).

Overall, these results suggest that the dysregulation of parvalbumin, Tweak, Fn14, and the proposed metabolic effectors in SMA muscle during disease progression is most likely not denervation dependent.

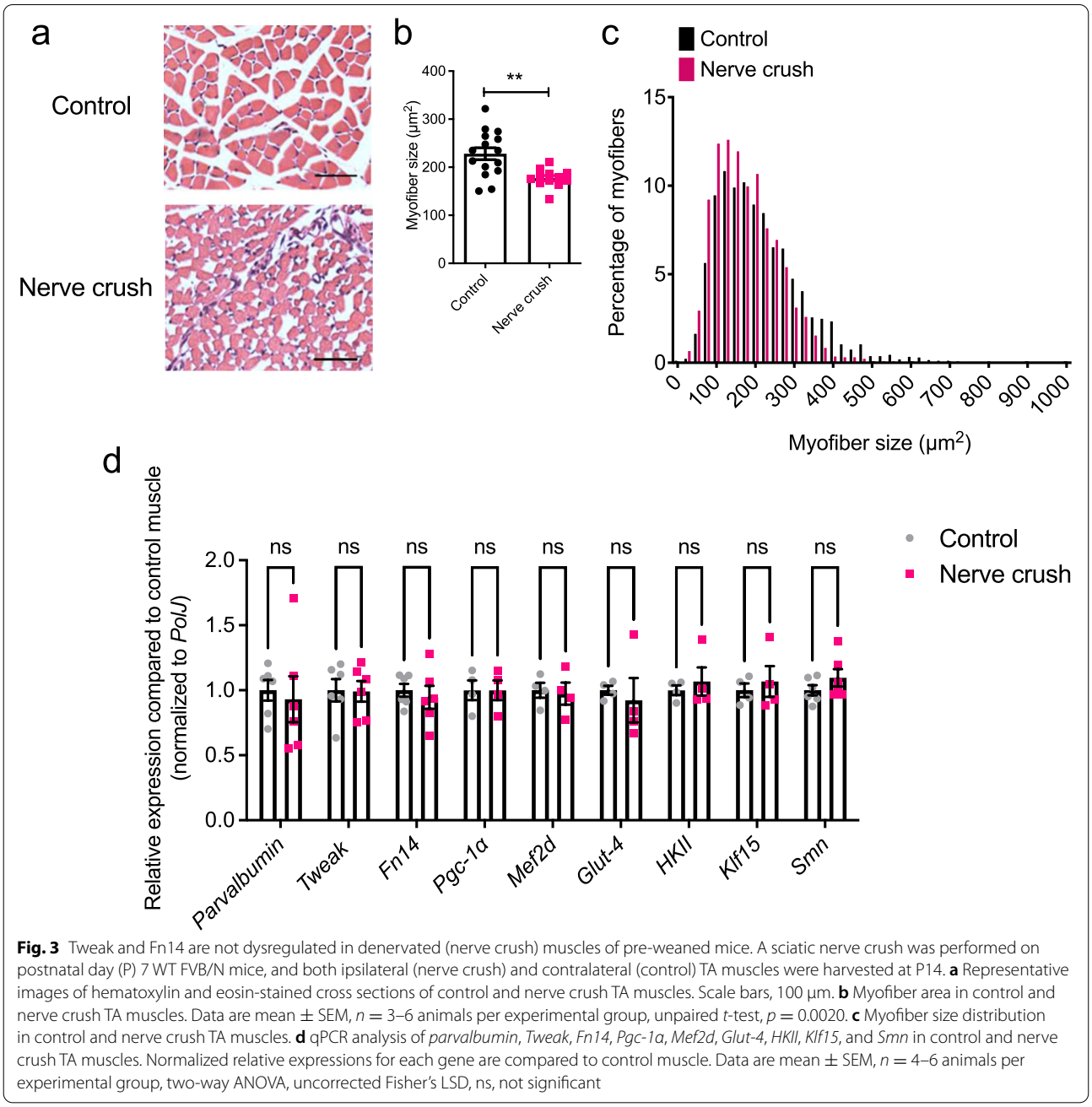

Fig. 3 Tweak and Fn14 are not dysregulated in denervated (nerve crush) muscles of pre-weaned mice. A sciatic nerve crush was performed on postnatal day (P) 7 WT FVB/N mice, and both ipsilateral (nerve crush) and contralateral (control) TA muscles were harvested at P14. **a** Representative images of hematoxylin and eosin-stained cross sections of control and nerve crush TA muscles. Scale bars, 100 μm. **b** Myofiber area in control and nerve crush TA muscles. Data are mean ± SEM, $n = 3$–6 animals per experimental group, unpaired *t*-test, $p = 0.0020$. **c** Myofiber size distribution in control and nerve crush TA muscles. **d** qPCR analysis of *parvalbumin*, *Tweak*, *Fn14*, *Pgc-1a*, *Mef2d*, *Glut-4*, *HKII*, *Klf15*, and *Smn* in control and nerve crush TA muscles. Normalized relative expressions for each gene are compared to control muscle. Data are mean ± SEM, $n = 4$–6 animals per experimental group, two-way ANOVA, uncorrected Fisher's LSD, ns, not significant

Intrinsic muscle injury affects Tweak and Fn14 during the early stages of muscle development

We next investigated what impact impairing intrinsic muscle integrity would have on Tweak and Fn14. To do so, we used cardiotoxin to induce myofiber necrosis. Cardiotoxin was injected in P10 WT mice into the left TA, while the right TA was injected with equal volumes of 0.9% saline and used as a control. TAs were harvested after 6 days, a time point where muscles are still in an immature and regenerating mode [47]. Indeed, analysis of centrally located nuclei showed a significantly increased percentage of regenerating myofibers in cardiotoxin-treated muscles compared to saline-treated TAs (Fig. 4a–b).

We then proceeded with molecular analyses and observed that the atrophy marker *parvalbumin* was significantly downregulated in cardiotoxin-treated TA muscles compared to saline-treated TA muscles (Fig. 4c). *Fn14* mRNA expression was significantly increased after cardiotoxin injury (Fig. 4c), in accordance with previous research showing that muscle damage conditions activate Fn14 [15]. Conversely, *Pgc-1α*, *Glut-4*, *HKII* and *Klf15* mRNA levels were significantly downregulated (Fig. 4c), supporting their previously reported negative response to

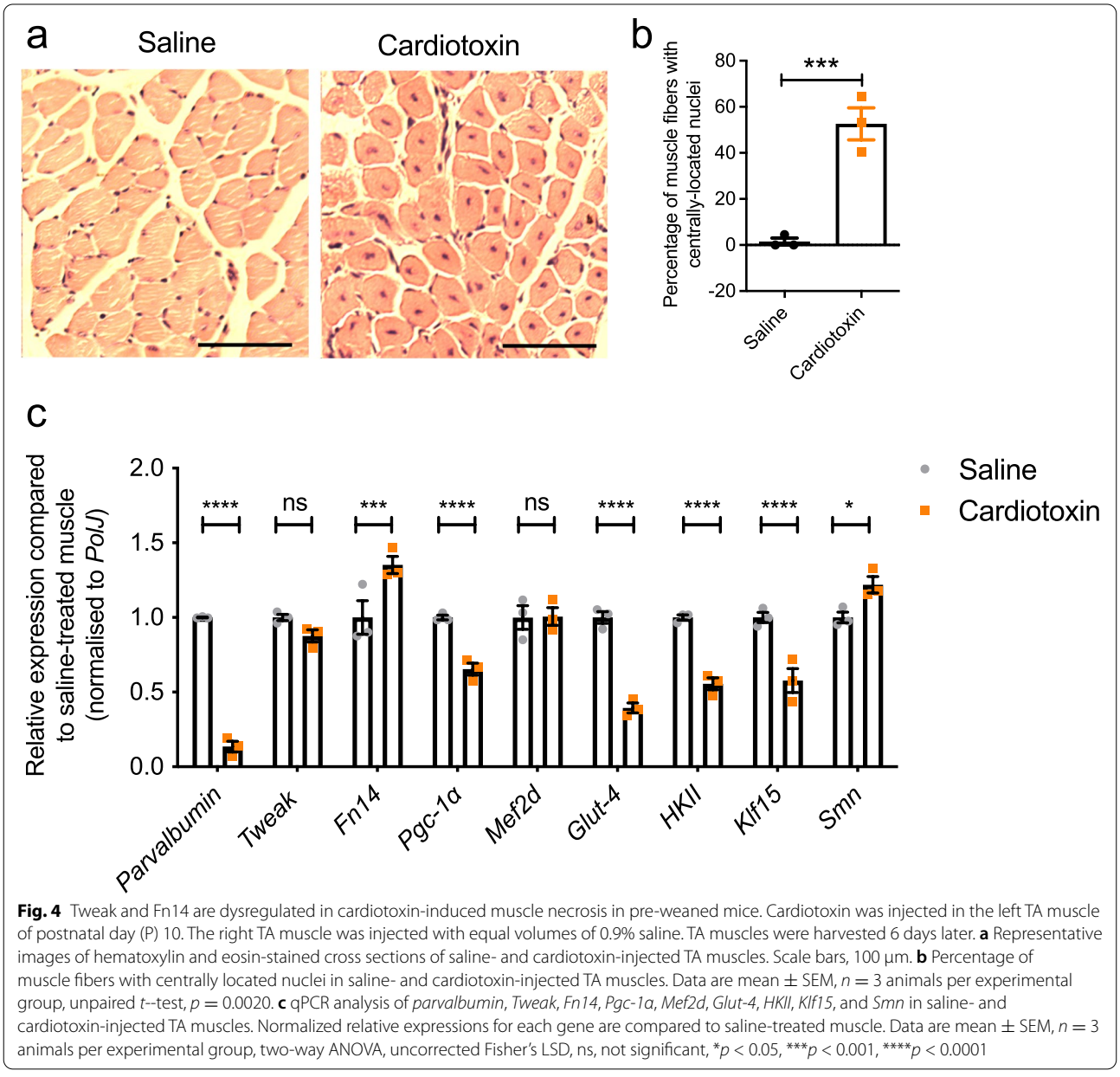

Fig. 4 Tweak and Fn14 are dysregulated in cardiotoxin-induced muscle necrosis in pre-weaned mice. Cardiotoxin was injected in the left TA muscle of postnatal day (P) 10. The right TA muscle was injected with equal volumes of 0.9% saline. TA muscles were harvested 6 days later. **a** Representative images of hematoxylin and eosin-stained cross sections of saline- and cardiotoxin-injected TA muscles. Scale bars, 100 µm. **b** Percentage of muscle fibers with centrally located nuclei in saline- and cardiotoxin-injected TA muscles. Data are mean ± SEM, $n = 3$ animals per experimental group, unpaired *t*--test, $p = 0.0020$. **c** qPCR analysis of *parvalbumin*, *Tweak*, *Fn14*, *Pgc-1a*, *Mef2d*, *Glut-4*, *HKII*, *Klf15*, and *Smn* in saline- and cardiotoxin-injected TA muscles. Normalized relative expressions for each gene are compared to saline-treated muscle. Data are mean ± SEM, $n = 3$ animals per experimental group, two-way ANOVA, uncorrected Fisher's LSD, ns, not significant, $^{*}p < 0.05$, $^{***}p < 0.001$, $^{****}p < 0.0001$

active Tweak and Fn14 [18]. Interestingly, *Tweak* mRNA expression remained unchanged (Fig. 4c), contrary to previous reports of upregulation following cardiotoxin injury in adult muscle [48], suggesting a differential response in early developmental stages of skeletal muscle. Notably, *Smn* expression was significantly increased in the regenerating muscles compared to saline-treated TA muscles (Fig. 4c), perhaps due to SMN's reported role during muscle fiber regeneration [49].

Together, these results suggest that intrinsic muscle injury in pre-weaned mice induces a dysregulation of Tweak, Fn14 and previously reported proposed metabolic effectors. However, the changes were in the opposite direction than that observed in SMA muscles (Fig. 1b), perhaps due to the necrosis and regeneration events that occur following cardiotoxin injury [50], which are not typically found in muscles of SMA mice.

Genetic interactions between Smn, Tweak, and Fn14 in muscle

We next wanted to further understand the potential relationship between dysregulated expression of *Tweak*, *Fn14*, and *Smn* in skeletal muscle of SMA mice. To do so, we evaluated the impact of Tweak and Fn14 depletion in the early stages of muscle development by performing molecular analyses on P7 triceps from $Fn14^{-/-}$, $Tweak^{-/-}$ and WT mice. In $Tweak^{-/-}$ mice, we observed a significant increased expression of *Fn14* with a concomitant significantly decreased expression of *Klf15* compared to WT animals (Fig. 5a). Notably, we found a significant decreased expression of *Smn* in $Tweak^{-/-}$ triceps compared to WT mice (Fig. 5a), suggesting a direct or indirect positive interaction between Tweak and Smn levels. For their part, $Fn14^{-/-}$mice displayed a significant downregulation of *parvalbumin* and a significant upregulation of *Pgc-1α* (Fig. 5b). These analyses further support the previously reported negative influence of Fn14 on Pgc-1α and Klf15 expression as well as the absence of overt pathological muscle phenotypes in young $Tweak^{-/-}$ and $Fn14^{-/-}$ mice [15, 51].

To further dissect the relationship between Smn, Tweak, and Fn14 during myogenic differentiation, we performed siRNA-mediated knockdown of *Smn*, *Tweak* and *Fn14* in C2C12 myoblasts and evaluated the effect on the expression of Tweak, Fn14, and the previously reported proposed metabolic effectors in undifferentiated (day 0) and differentiated (day 7) cells. Reduced levels of *Smn*, *Tweak* and *Fn14* were significantly maintained in both proliferating and differentiated cells following transfection with *siSmn*, *siTweak*, and *siFn14*, respectively (Fig. 5c–e). We observed an interaction between *Smn*, *Tweak* and *Fn14* specifically in differentiated C2C12s, whereby *Smn* expression was significantly upregulated in *Fn14*-depleted D7 cells (Fig. 5c), *Tweak* expression was significantly reduced in *Smn*-depleted D7 cells (Fig. 5d) and *Fn14* levels were significantly decreased in *Tweak*- and *Smn*-depleted D7 cells (Fig. 5e). Similarly, the effects of siRNA-mediated knockdown of *Smn*, *Tweak* and *Fn14* on the metabolic effectors were only apparent in differentiated C2C12s (Fig. 5f–j). Indeed, both knockdown of *Tweak* and *Fn14* resulted in a significant upregulation of *Pgc-1α* (Fig. 5f) and *Mef2d* (Fig. 5g). While *Glut-4* expression was neither affected by depletion of *Smn*, *Tweak*, or *Fn14* (Fig. 5h), *HKII* mRNA levels were significantly decreased following knockdown of all three (Fig. 5i). Finally, *Klf15* expression was significantly increased in siRNA-mediated knockdown of *Fn14* only (Fig. 5j). The upregulation of *Pgc-1α*, *Mef2d* and *Klf15* in *Tweak*- and/or *Fn14*-depleted differentiated C2C12 cells is in accordance with the previously reported downregulation of these genes when Tweak and Fn14 are active, while the unchanged *Glut-4* and downregulated *HKII* levels were not [52].

Thus, using both in vivo and in vitro models, we have provided evidence for a potential interaction between *Smn*, *Tweak* and *Fn14* and subsequent impact on the previously proposed downstream metabolic effectors (Fig. 5k). Our results suggest that the aberrant expression of Tweak and Fn14 in SMA muscle during disease progression may be due to a dynamic interplay between muscle-specific conditions and the molecular impact, individual and combined, of reduced expression of Smn, Tweak and Fn14 in the early developmental stages of skeletal muscle.

(See figure on next page.)

Fig. 5 *Smn*, *Tweak*, and *Fn14* depletion impact each other's expression. **a**–**b** qPCR analysis of *parvalbumin*, *Tweak*, *Fn14*, *Pgc-1α*, *Mef2d*, *Glut-4*, *HKII*, *Klf15*, and *Smn* in triceps muscle from postnatal day (P) 7 $Tweak^{-/-}$ (**a**) and $Fn14^{-/-}$ (**b**) mice. Normalized relative expressions for each gene are compared to WT. Data are mean ± SEM, $n = 4$ animals per experimental group, two-way ANOVA, uncorrected Fisher's LSD, *ns*, not significant, *$p < 0.05$, ***$p < 0.001$, ****$p < 0.0001$. **c**–**j** qPCR analysis of *Smn* (**c**), *Tweak* (**d**), *Fn14* (**e**), *Pgc-1α* (**f**), *Mef2d* (**g**), *Glut-4* (**h**), *HKII* (**i**), and *Klf15* (**j**) in siRNA-mediated *Tweak*-, *Fn14*-, and *Smn*-depleted and control proliferating (day 0) and differentiated (day 7) C2C12 cells. Normalized relative expressions for day 1 experimental groups are compared to day 1 untreated group, and normalized relative expressions for day 7 experimental groups are compared to day 7 untreated group. Data are mean ± SEM, $n = 3$ per experimental group, two-way ANOVA, Dunnett's multiple comparisons test, *$p < 0.05$, **$p < 0.01$, ***$p < 0.001$, ****$p < 0.0001$. **k** Proposed model of the relationship between Smn and the Tweak/Fn14 signaling pathway. Red lines represent inhibition, and blue lines represent activation

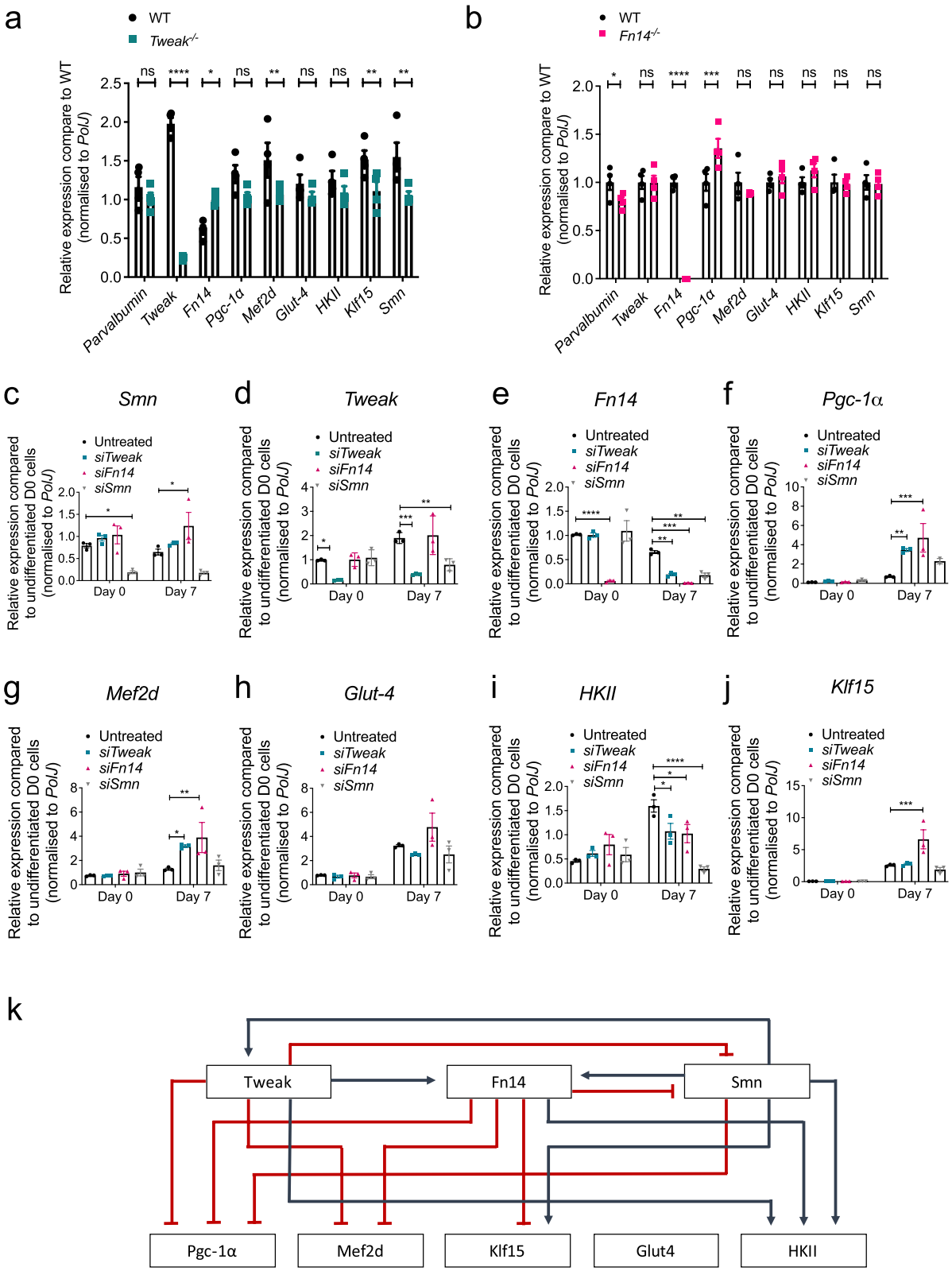

Fig. 5 (See legend on previous page.)

Overlap of dysregulated myopathy and myogenesis genes and glucose metabolism genes in SMA, Fn14$^{-/-}$ and Tweak$^{-/-}$ mice

To further decipher the potential contribution(s) of Smn, Tweak, and Fn14 depletion to SMA muscle pathology, we used commercially available mouse myopathy and myogenesis qPCR arrays (SABiosciences), which measure expression levels of a subset of 84 genes known to display and/or regulate myopathy and myogenesis. We used triceps (vulnerable) and quadriceps (resistant) from P7 *Smn*$^{-/-}$*;SMN2*, *Tweak*$^{-/-}$and *Fn14*$^{-/-}$ mice. WT FVB/N mice were compared to SMA animals and WT C57BL/6 mice were compared to *Tweak*$^{-/-}$ and *Fn14*$^{-/-}$ mice to account for differences due to genetic strains. Unsurprisingly, we observed a larger number of significantly dysregulated myopathy and myogenesis genes in triceps of *Smn*$^{-/-}$*;SMN2* mice than in the more resistant quadriceps, some of which overlapped with the subset of genes aberrantly expressed in *Fn14*$^{-/-}$ mice and *Tweak*$^{-/-}$ mice (Fig. 6a, Table 1, Supplementary file 1). We also used the publicly available database STRING [34] to perform network and enrichment analysis of the shared differentially expressed genes in both triceps and quadriceps (Table 1), which revealed that there were no known protein-protein interactions between any of the dysregulated genes and Smn, Fn14, or Tweak (Fig. 6b). Interestingly, the central connectors *Myod1* and *Myf6* were upregulated in *Tweak*$^{-/-}$ and *Fn14*$^{-/-}$ mice and *Pax7* was downregulated in the triceps of all three experimental groups (Table 1). Myod1 and Myf6 are key myogenic regulatory factors (MRFs) and are normally upregulated after skeletal muscle injury [53]. Pax7 is a canonical marker for satellite cells, the resident skeletal muscle stem cells [53], and reduced activity of Pax7 leads to cell-cycle arrest of satellite cells and dysregulation of MRFs in skeletal muscle [54]. Furthermore, *Titin* (*Ttn*) was downregulated in the quadriceps muscles of all three mouse models and plays major roles in muscle contraction and force production, highlighted by titin mutations leading to a range of skeletal muscle diseases and phenotypes [55].

Next, as SMN, TWEAK, and Fn14 have been associated with glucose metabolism abnormalities [18, 56], we performed similar gene expression analyses with commercially available qPCR arrays (SABiosciences) containing a subset of 84 genes known to display and/or regulate glucose metabolism. We found a similar large number of genes that were dysregulated in both triceps and quadriceps muscles of *Smn*$^{-/-}$*;SMN2* mice, some of which overlapped with those differentially expressed in *Fn14*$^{-/-}$ and *Tweak*$^{-/-}$ mice (Fig. 6c, Table 2, Supplementary file 2). STRING network and enrichment analysis [34] revealed that there are no known protein-protein interactions between any of the dysregulated genes and Smn, Fn14, or Tweak (Fig. 6d). Further analysis of the Kyoto Encyclopedia of Genes and Genomes (KEGG) pathways composed of the glucose metabolism genes significantly dysregulated in the same direction in triceps and quadriceps muscles of P7 *Smn*$^{-/-}$*;SMN2*, *Fn14*$^{-/-}$ and *Tweak*$^{-/-}$ mice as well as the downstream effectors of the TWEAK/Fn14 pathway studied in this project (Pgc-1α, Mef2d, Glut4, Klf15 and HKII) reveals that many aspects of glucose metabolism such as insulin signaling and glycolysis are dysregulated in Smn-, Tweak-, and Fn14-depleted mice (Table 3).

We thus show a shared pattern of aberrantly expressed genes that modulate myogenesis, myopathy and glucose metabolism in SMA, Tweak-depleted, and Fn14-depleted skeletal muscle, suggesting that Smn, Tweak, and Fn14 may act synergistically on muscle pathology and metabolism defects in SMA muscle.

(See figure on next page.)

Fig. 6 Overlap between dysregulated genes involved in myopathy, myogenesis, and glucose metabolism in skeletal muscle of *Smn*$^{-/-}$*;SMN2*, *Fn14*$^{-/-}$, and *Tweak*$^{-/-}$ mice. **a** Venn diagram showing overlap of genes involved in myopathy and myogenesis that are significantly dysregulated in the same direction (either up or downregulated, $p < 0.05$) in triceps and quadriceps muscle from postnatal day (P) 7 compared to *Smn*$^{-/-}$*;SMN2*, *Fn14*$^{-/-}$, and *Tweak*$^{-/-}$ mice to age- and genetic strain-matched wild-type (WT) mice. **b** Network and enrichment analysis of the overlap of significantly dysregulated myopathy and myogenesis genes in triceps and/or quadriceps of P7 *Smn*$^{-/-}$*;SMN2*, *Fn14*$^{-/-}$, and *Tweak*$^{-/-}$ mice using STRING software. Smn (Smn1), TWEAK (Tnfsf12), and Fn14 (Tnfrsf12a) are included in the analysis. Colored nodes represent query proteins and first shell of interactors. Filled nodes indicate that some 3D structure is known or predicted. Connection colored lines between nodes represent either known interactions (turquoise: from curated databases, magenta: experimentally determined), predicted interactions (green: gene neighborhood, red: gene fusions, dark blue: gene co-occurrence) or other interactions (yellow: textmining, black: co-expression, light blue: protein homology). **c** Venn diagram showing overlap of genes involved in glucose metabolism that is significantly dysregulated in the same direction (either up or downregulated, $p < 0.05$) in triceps and quadriceps muscle from P7 compared to *Smn*$^{-/-}$*;SMN2*, *Fn14*$^{-/-}$, and *Tweak*$^{-/-}$ mice to age- and genetic strain-matched WT mice. **d** Network and enrichment analysis of the overlap of significantly dysregulated myopathy and myogenesis genes in triceps and/or quadriceps of P7 *Smn*$^{-/-}$*;SMN2*, *Fn14*$^{-/-}$, and *Tweak*$^{-/-}$ mice using STRING software. Smn (Smn1), TWEAK (Tnfsf12), Fn14 (Tnfrsf12a), HKII (Hk2), Glut4 (Slc2a4), Pgc-1α (Ppargc1a), Klf15, and Mef2d are included in the analysis. Colored nodes represent query proteins and first shell of interactors. Filled nodes indicate that some 3D structure is known or predicted. Connection colored lines between nodes represent either known interactions (turquoise: from curated databases, magenta: experimentally determined), predicted interactions (green: gene neighborhood, red: gene fusions, dark blue: gene co-occurrence) or other interactions (yellow: textmining, black: co-expression, light blue: protein homology)

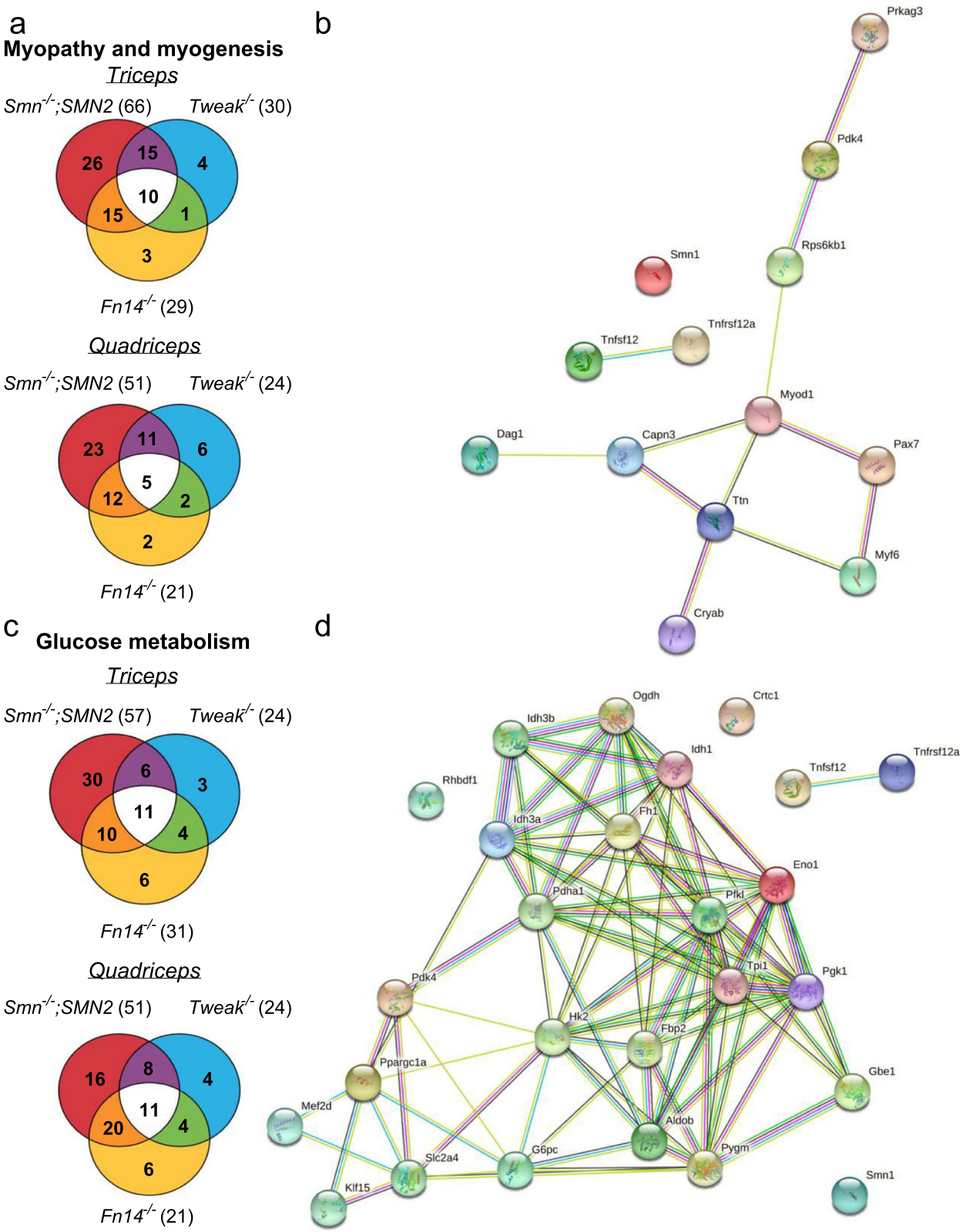

Fig. 6 (See legend on previous page.)

Table 1 Myogenesis and myopathy genes significantly dysregulated in the same direction in triceps and quadriceps of P7 *Smn*$^{-/-}$*;SMN2*, *Fn14*$^{-/-}$ and *Tweak*$^{-/-}$ mice when compared to P7 WT mice

		Triceps						*Quadriceps*					
		Smn$^{-/-}$*;SMN2*		*Fn14*$^{-/-}$		*Tweak*$^{-/-}$		*Smn*$^{-/-}$*;SMN2*		*Fn14*$^{-/-}$		*Tweak*$^{-/-}$	
Gene		***Fold change***	***p-value***	***Fold change***	***p-value***	***Fold change***	***p-value***	***Fold change***	***p-value***	***Fold change***	***p-value***	***Fold change***	***p-value***
Crystallin alpha B (Cryab)	**Up**	1.3245	0.002813	1.3814	0.010565	1.3711	0.041543	1.386	0.013894	1.2332	0.000616		*ns*
Dystroglycan 1 (Dag1)	**Down**	↑		−1.1823	0.008415	−1.3607	0.001058	−1.3575	0.039065	−1.1416	0.003343	−1.4885	0.001277
Insulin-like growth factor binding protein 5 (Igfbp5)	**Down**	-6.5548	0	−1.6343	0.000135	−1.2758	0.008243	−8.0095	0.000017	−1.2813	0.006583		*ns*
Myogenic factor 6 (Myf6)	**Up**	↓		1.1221	0.008823	1.6485	0.003036	1.0137	0.831317		*ns*	1.4051	0.006745
Myogenic differentiation 1 (Myod1)	**Up**	↓		1.2595	0.046953	1.91	0.000369	↓			*ns*		*ns*
Paired Box 7 (Pax7)	**Down**	−1.7035	0.000189	−1.1814	0.001774	−1.1522	0.014681	−2.4268	0.000151		*ns*		*ns*
Protein kinase AMP-activated non-catalytic subunit gamma 3 (Prkag3)	**Down**	−13.700	0	−1.7401	0.002101	−1.6191	0.001641	−8.0475	0.000019	−1.6521	0.005939	−1.6346	0.006477
Pyruvate dehydrogenase kinase 4 (Pdk4)	**Up**	7.7734	0.005328	1.8326	0.01063	2.209	0.004106	5.3978	0.055184	1.9628	0.006922	1.5978	0.003346
Ribosomal protein S6 kinase B1 (Rps6kb1)	**Down**	−1.1105	0.045173	−1.1183	0.012509	−1.335	0.006426	−1.541	0.012036	−1.1078	0.027897	−1.4257	0.000143
Titin (Ttn)	**Down**	−1.4206	0.000015	−1.1322	0.023526		*ns*	−1.8247	0.000386	−1.1965	0.01243	−1.2861	0.001181

Ns not significant, ↑significantly upregulated, ↓significantly downregulated. Fold change (2^(-delta-delta CT)) is the normalized gene expression (2^(-delta CT)) in the test sample divided the normalized gene expression (2^(-delta CT)) in the WT samples. Fold-change values greater than 1 indicate a positive- or an upregulation and the fold regulation is equal to the fold change. Fold-change values less than 1 indicate a negative or downregulation and the fold regulation is the negative inverse of the fold change. The *p*-values are calculated based on a Student's *t*-test of the replicate 2^(-delta CT) values for each gene in the control group and treatment groups

Table 2 Glucose metabolism genes significantly dysregulated in the same direction in triceps and quadriceps of P7 *Smn*$^{-/-}$;*SMN2*,$^{-}$*Fn14*$^{-/-}$ and *Tweak*$^{-/-}$ mice when compared to P7 WT mice

Gene		*Triceps*						*Quadriceps*					
		Smn$^{-/-}$;*SMN2*		*Fn14*$^{-/-}$		*Tweak*$^{-/-}$		*Smn*$^{-/-}$;*SMN2*		*Fn14*$^{-/-}$		*Tweak*$^{-/-}$	
		Fold change	*p-value*	*Fold change*	*p-value*	*Fold change*	*p-value*	*Fold change*	*p-value*	*Fold change*	*p-value*	*Fold change*	*p-value*
1,4-Alpha-glucan branching enzyme 1 (Gbe1)	**Down**	1.2158	0.001826	−1.1649	0.00362		*ns*	↑		−1.3664	0.00073	−1.648	0.002807
Dihydrolipoamide S-succinyltransferase (Dlst)	**Down**	−1.4834	0.000409	−1.1593	0.000992	−1.5512	0.009639	−1.7555	0.000001	−1.2472	0.000422	−1.4384	0.000389
Enolase 1 (Eno1)	**Down**	−2.8937	0	−1.2057	0.001592	−1.2553	0.012037	−2.8182	0	−1.3798	0.000748	−1.6093	0.000595
Filamin B (Fh1)	**Down**	−1.2988	0.002491	−1.11	0.011675	−1.2603	0.044285	−1.4732	0.000033	−1.1362	0.010963		*ns*
Fructose-bisphosphatase 2 (Fbp2)	**Up**	1.3862	0.002522	1.6462	0.003035	1.4036	0.004574	1.5193	0.000348	1.4564	0.00028		*ns*
Glycogen hosphorylase muscle-associated (Pygm)	**Down**	−1.2185	0.002346		*ns*		*ns*	−1.2577	0.000493	−1.1492	0.034146	−1.1388	0.045356
Isocitrate dehydrogenase 3 (NAD(+)) alpha (Idh3a)	**Down**	−1.3412	0.014566	−1.0994	0.022547	−1.2728	0.007865	−1.6021	0.000063	−1.3412	0.002972	−1.288	0.023111
Isocitrate dehydrogenase 3 (NAD(+)) Beta (Idh3b)	**Down**	−1.2006	0.00032	−1.1227	0.017864		*ns*	−1.3376	0.00003	−1.1815	0.001146	−1.1462	0.018887
Oxoglutarate dehydrogenase (Ogdh)	**Down**	−1.184	0.032659	−1.0914	0.009317	−1.3354	0.001844	−1.295	0.000068	−1.2062	0.010753	−1.4183	0.011564
Phosphofructokinase, liver type (Pfkl)	**Down**	−1.3403	0.002443		*ns*		*ns*	−1.8003	0.033611	−1.2159	0.003577	−1.699	0.00477
Pyruvate dehydrogenase E1 alpha 1 subunit (Pdha1)	**Down**		*ns*	−1.1094	0.005985	−1.1421	0.040785	−1.1915	0.029091	−1.2056	0.006742	−1.2258	0.009299
Pyruvate dehydrogenase kinase 4 (Pdk4)	**Up**	7.4434	0.002676	1.6982	0.017988	1.7597	0.03066	5.3286	0.038343	1.7406	0.003824	1.556	0.006172
Phosphoglycerate kinase 1 (Pgk1)	**Down**	−1.7093	0.000041	−1.1129	0.006326	−1.1699	0.049145	−1.7605	0	−1.3544	0.006063		*ns*
Triosephosphate isomerase 1 (Tpi1)	**Down**	−1.8595	0.000342		*ns*		*ns*	−1.8225	0.000006	−1.2313	0.002462	−1.2697	0.011066

Ns not significant, ↑ significantly upregulated. Fold change (2^(-delta-delta CT)) is the normalized gene expression (2^(-delta CT)) in the test sample divided the normalized gene expression (2^(-delta CT)) in the WT samples. Fold-change values greater than 1 indicate a positive- or an upregulation and the fold regulation is equal to the fold change. Fold-change values less than 1 indicate an negative or downregulation and the fold regulation is the negative inverse of the fold change. The *p*-values are calculated based on a Student's *t*-test of the replicate 2^(-delta CT) values for each gene in the control group and treatment groups

Table 3 KEGG pathways generated from glucose metabolism genes that were significantly dysregulated in the same direction in triceps and quadriceps of P7 *Smn*$^{-/-}$*;SMN2*, *Fn14*$^{-/-}$ and *Tweak*$^{-/-}$ mice when compared to P7 WT mice

Pathway ID	Pathway description	Count in gene set	False discovery rate (FDR)
01200	Carbon metabolism	13	7.62e-22
01120	Microbial metabolism in diverse environments	13	1.87e-19
00010	Glycolysis/Gluconeogenesis	8	2.09e-13
00020	Citrate cycle (TCA cycle)	7	2.09e-13
01100	Metabolic pathways	16	7.65e-13
01230	Biosynthesis of amino acids	7	8.75e-11
00051	Fructose and mannose metabolism	5	1.7e-08
04910	Insulin signaling pathway	6	3.09e-07
00500	Starch and sucrose metabolism	4	8.58e-06
04152	AMPK signaling pathway	5	8.58e-06
01210	2-Oxocarboxylic acid metabolism	3	2.79e-05
00030	Pentose phosphate pathway	3	0.000126
04066	HIF-1 signaling pathway	4	0.000141
00052	Galactose metabolism	3	0.000145
04920	Adipocytokine signaling pathway	3	0.00138
00620	Pyruvate metabolism	2	0.0177
04973	Carbohydrate digestion and absorption	2	0.0177
04930	Type II diabetes mellitus	2	0.0227
00310	Lysine degradation	2	0.0233

Administration of the Fc-TWEAK agonist improves a subset of disease phenotypes in two SMA mouse models

Finally, we evaluated the impact of increasing Tweak activity on disease progression and muscle pathology in SMA mice.

Of note, while the *Smn*$^{+/-}$*;SMN2* and *Smn*$^{2B/+}$ mice are healthy littermates in terms of life span and reproductive abilities, they nevertheless have reduced levels of Smn, which in itself has been demonstrated to impact certain phenotypic features (e.g., tail and ear necrosis, metabolism, gene expression). As such, and similar to previous studies [41], comparisons were performed between untreated and treated animals of the same genotype, allowing us to determine if the effects were SMA-dependent and/or -independent, without the addition of a potential compounding factor.

Firstly, *Smn*$^{-/-}$*;SMN2* mice and healthy littermates received a daily subcutaneous injection of Fc-TWEAK (15.8 µg), a fusion protein with the murine IgG2a Fc region [26], starting at birth. We found that Fc-TWEAK did not significantly impact weight or survival of *Smn*$^{-/-}$*;SMN2* mice compared to untreated and IgG-treated controls (Fig. 7a–b). Additional lower (7.9 µg) and higher doses (23 and 31.6 µg) were also administered but proved to negatively impact weight and survival (Supplementary Fig. 3).

Triceps from P7-untreated and Fc-TWEAK-treated (15.8 µg) *Smn*$^{-/-}$*;SMN2* SMA mice and *Smn*$^{+/-}$*;SMN2* healthy littermates were further processed for molecular analyses of the Tweak/Fn14 pathway. We observed that Fc-TWEAK administration did not influence the expression of *Tweak* (Fig. 7c) or *Fn14* (Fig. 7d) in neither *Smn*$^{+/-}$*;SMN2* nor *Smn*$^{-/-}$*;SMN2* mice compared to untreated animals. Similarly, Fc-TWEAK did not induce changes in *Pgc-1α* expression (Fig. 7e). We did observe a significant downregulation of *Mef2d* in Fc-TWEAK-treated muscles of *Smn*$^{-/-}$*;SMN2* SMA mice compared to untreated animals (Fig. 7f). *Glut-4* mRNA expression remained unchanged in both *Smn*$^{+/-}$*;SMN2* and *Smn*$^{-/-}$*;SMN2* Fc-TWEAK-treated mice (Fig. 7g). *HKII* was significantly upregulated in muscle of Fc-TWEAK-treated *Smn*$^{+/-}$*;SMN2* healthy littermates, while it was significantly downregulated in Fc-TWEAK-treated *Smn*$^{-/-}$*;SMN2* SMA mice compared to untreated groups (Fig. 7h). *Klf15* was significantly downregulated in Fc-TWEAK-treated *Smn*$^{-/-}$*;SMN2* SMA mice only compared to untreated SMA animals (Fig. 7i). The absence of overt changes in the expression of Tweak, Fn14 and the previously reported proposed downstream metabolic effectors may be due to the 24-h time-lapse between the last Fc-TWEAK injection and harvest of tissues, which could have led to missing key time points at which transcriptional profiles were significantly impacted.

While we did not capture the short-term molecular effects of Fc-TWEAK administration, quantification of myofiber area in TA muscles showed that daily Fc-TWEAK treatment significantly increased myofiber area in skeletal muscle of P7 *Smn*$^{-/-}$*;SMN2* mice compared to untreated SMA animals (Fig. 7j–k). Furthermore, the expression of atrophy markers *parvalbumin*, *MuRF-1* and *atrogin-1* [57] was also restored towards normal levels, whereby *parvalbumin* expression was significantly increased (Fig. 7l), while *MuRF-1* and *atrogin-1* expression was significantly downregulated (Fig. 7m–n) in triceps of Fc-TWEAK-treated *Smn*$^{-/-}$*;SMN2* SMA mice compared to untreated SMA animals, further supporting an improvement in muscle health. We did not however detect changes in MRFs *Myod1* and *myogenin* [53] (Fig. 7o–p).

We next assessed the effect of Fc-TWEAK in *Smn*$^{2B/-}$ mice, which are typically more responsive to Smn-independent treatment strategies [41, 58–60]. Due to the longer treatment period in these mice (20 days) and the observed toxicity in daily injected mice (> 10 days), the *Smn*$^{2B/-}$ and *Smn*$^{2B/+}$ mice received subcutaneous injections of Fc-TWEAK and IgG control (15.8 µg) every 4 days, starting at birth. Both IgG and Fc-TWEAK did not significantly impact the weight of *Smn*$^{2B/-}$ mice compared to untreated SMA animals (Fig. 7q). However, Fc-TWEAK significantly increased the lifespan of *Smn*$^{2B/-}$ mice compared to both IgG-treated and untreated animals (Fig. 7r). Molecular analyses of the mRNA levels of *Tweak*, *Fn14* and the previously reported proposed molecular effectors in triceps from P15 animals only showed a significant effect of Fc-TWEAK on the expression of *Glut-4*, whereby it was downregulated in Fc-TWEAK-treated *Smn*$^{2B/-}$ mice compared to untreated animals (Fig. 7s). Similar to the above, the limited impact of Fc-TWEAK on the expression of Tweak, Fn14 and the previously reported metabolic effectors in P15 animals may be due to the 72-h time-lapse between the last injection of Fc-TWEAK and tissue harvest. This experimental paradigm was chosen to follow the optimal dosing regimen and perform molecular analyses at a symptomatic time-point that was not too close to the end stage of the disease. Nevertheless, to determine if molecular changes could be captured following a shorter time-lapse between the Fc-TWEAK injection and tissue harvest and to determine if the response to Fc-TWEAK is different in WT tissues that express 100% Smn, we treated WT and *Smn*$^{2B/-}$ with Fc-TWEAK (15.8 µg) every 4 days from birth until P16 and harvested skeletal muscle 3-h post-injection. While *Fn14* mRNA expression remained unchanged in the triceps from both WT and SMA mice (Supplementary Fig. 4a), we found differential expression

(See figure on next page.)

Fig. 7 Increasing Tweak activity via Fc-TWEAK improves disease phenotypes in two SMA mouse models. **a** Daily weights of untreated *Smn*$^{-/-}$*;SMN2* SMA mice and *Smn*$^{-/-}$*;SMN2* mice that received daily subcutaneous injections (starting at P0) of Fc-TWEAK or IgG control (15.8 µg). Data are mean ± SEM, $n = 7$–10 animals per experimental group, two-way ANOVA, Sidak's multiple comparison test. **b** Survival curves of untreated *Smn*$^{-/-}$*;SMN2* SMA mice and *Smn*$^{-/-}$*;SMN2* that received daily subcutaneous injections of Fc-TWEAK or IgG control (15.8 µg). Data are represented as Kaplan-Meier survival curves, $n = 7$–10 animals per experimental group, log-rank (Mantel-Cox). **c**–**i**. qPCR analysis of *Tweak* (**c**), *Fn14* (**d**), *Pgc-1α* (**e**), *Mef2d* (**f**), *Glut-4* (**g**), *HKII* (**h**), and *Klf15* (**i**) in triceps of postnatal day (P) 7 untreated and Fc-TWEAK-treated (15.8 µg) *Smn*$^{-/-}$*;SMN2* SMA and *Smn*$^{+/-}$*;SMN2* health littermates. Normalized relative expressions for Fc-TWEAK-treated *Smn*$^{+/-}$*;SMN2* mice are compared to untreated *Smn*$^{+/-}$*;SMN2* mice, and normalized relative expressions for Fc-TWEAK-treated *Smn*$^{-/-}$*;SMN2* mice are compared to untreated *Smn*$^{-/-}$*;SMN2* mice. Data are mean ± SEM, $n = 3$–4 animals per experimental group, two-way ANOVA, uncorrected Fisher's LSD between genotypes, *$p < 0.05$, ***$p < 0.001$. **j** Representative images of laminin-stained cross sections of TA muscles from P7-untreated and Fc-TWEAK-treated (15.8 µg) *Smn*$^{-/-}$*;SMN2* SMA and *Smn*$^{+/-}$*;SMN2* health littermates (Scale bars = 100 µm) and quantification of myofiber area. Data are mean ± SEM, $n = 3$–4 animals per experimental group (> 550 myofibers per experimental group), one-way ANOVA, Tukey's multiple comparison test, *$p < 0.05$, ****$p < 0.0001$. **k** Relative frequency distribution of myofiber size in TA muscles of P7-untreated and Fc-TWEAK-treated (15.8 µg) *Smn*$^{-/-}$*;SMN2* SMA and *Smn*$^{+/-}$*;SMN2* health littermates. **l**–**p** qPCR analysis of *parvalbumin* (**l**), *MuRF-1* (**m**), *atrogin-1* (**n**), *Myod1* (**o**), and *myogenin* (**p**) in triceps of P7-untreated and Fc-TWEAK-treated (15.8 µg) *Smn*$^{-/-}$*;SMN2* SMA and *Smn*$^{+/-}$*;SMN2* health littermates. Normalized relative expressions for Fc-TWEAK-treated *Smn*$^{+/-}$*;SMN2* mice are compared to untreated *Smn*$^{+/-}$*;SMN2* mice, and normalized relative expressions for Fc-TWEAK-treated *Smn*$^{-/-}$*;SMN2* mice are compared to untreated *Smn*$^{-/-}$*;SMN2* mice. Data are mean ± SEM, $n = 3$–4 animals per experimental group, two-way ANOVA, uncorrected Fisher's LSD between genotypes, *$p < 0.05$, **$p < 0.01$. **q** Daily weights of untreated *Smn*$^{2B/-}$ SMA mice and *Smn*$^{2B/-}$ mice that received subcutaneous injections of Fc-TWEAK or IgG control (15.8 µg) every 4 days (starting at P0). Data are mean ± SEM, $n = 9$–12 animals per experimental group, two-way ANOVA, Sidak's multiple comparison test. **r** Survival curves of untreated *Smn*$^{2B/-}$ SMA mice and *Smn*$^{2B/-}$ mice that received subcutaneous injections of Fc-TWEAK or IgG control (15.8 µg) every 4 days (starting at P0). Data are Kaplan-Meier survival curves, $n = 9$–12 animals per experimental group, log-rank (Mantel-Cox), $p = 0.0162$. **s**–**x**. qPCR analysis of *Glut-4* (**s**), *parvalbumin* (**t**), *MuRF-1* (**u**), *atrogin-1* (**v**), *Myod1* (**w**), and *myogenin* (**x**) in P15 untreated and Fc-TWEAK-treated (15.8 µg) *Smn*$^{2B/+}$ and *Smn*$^{2B/-}$ mice (every 4 days starting at P0). Normalized relative expressions for Fc-TWEAK-treated *Smn*$^{2B/+}$ mice are compared to untreated *Smn*$^{2B/+}$ mice, and normalized relative expressions for Fc-TWEAK-treated *Smn*$^{2B/-}$ mice are compared to untreated *Smn*$^{2B/-}$ mice. Data are mean ± SEM, $n = 3$–4 animals per experimental group, two-way ANOVA, uncorrected Fisher's LSD between genotypes, *$p < 0.05$, ***$p < 0.001$, ns, not significant. **y** Representative images of laminin-stained cross sections of TA muscles from P16 untreated and Fc-TWEAK-treated (15.8 µg every 4 days starting at P0) *Smn*$^{2B/+}$ and *Smn*$^{2B/-}$mice (scale bars = 50 µm) and quantification of myofiber area. Data are mean ± SEM, $n = 3$–7 animals per experimental group (> 400 myofibers per experimental group), one-way ANOVA, Tukey's multiple comparison test, *$p < 0.05$, ****$p < 0.0001$. **z** Relative frequency distribution of myofiber size in TA muscles of P16 untreated and Fc-TWEAK-treated (15.8 µg every 4 days starting at P0) *Smn*$^{2B/+}$ and *Smn*$^{2B/-}$ mice

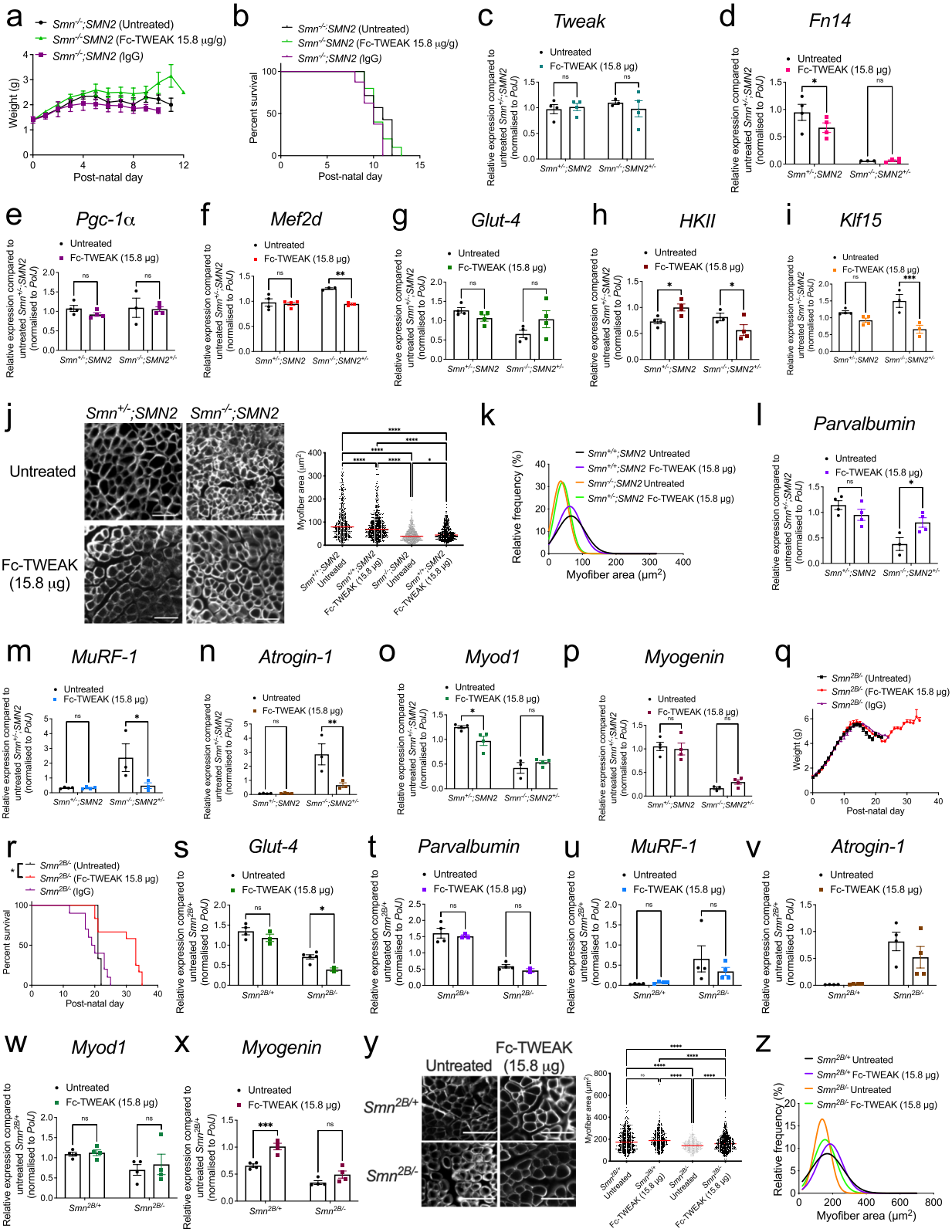

Fig. 7 (See legend on previous page.)

patterns of the other metabolic effectors proposed to be influenced by Tweak and Fn14. Indeed, following Fc-TWEAK injections, *Tweak* mRNA is significantly increased in WT animals and unchanged in $Smn^{2B/-}$ mice (Supplementary Fig. 4b). *PGC-1a* and *Mef2d* are unchanged in WT animals and significantly decreased in $Smn^{2B/-}$ mice (Supplementary Fig. 4 c–d), while *Glut-4*, *HKII* and *Klf15* are significantly increased in WT animals and significantly decreased in $Smn^{2B/-}$ animals (Supplementary Fig. 4 e–g). Similarly, we observed a specific decrease of the NF-κB2 p100 component (all other components were unchanged) in Fc-TWEAK-treated WT animals compared to untreated controls, while it is significantly upregulated in Fc-TWEAK-treated $Smn^{2B/-}$ mice compared to untreated animals (Supplementary Fig. 4h).

As improvements in muscle health parameters were observed in Fc-TWEAK-treated $Smn^{-/-}$;*SMN2* SMA mice, we performed similar investigations in $Smn^{2B/-}$ mice. Contrary to the more severe mouse model, we did not find any significant changes in expression levels of *parvalbumin*, *MuRF-1*, *atrogin-1* and *myod1* in neither $Smn^{2B/+}$ or $Smn^{2B/-}$ Fc-TWEAK-treated animals (Fig. 7t–w). We did observe a significant increase in *myogenin* mRNA expression that was limited to Fc-TWEAK-treated healthy littermates (Fig. 7x). These results suggest that the impact of Fc-TWEAK on molecular markers associated with muscle health may be dependent on age, disease severity and/or genetic strain. Despite the lack of impact of Fc-TWEAK on muscle atrophy and health markers, quantification of myofiber area in TA muscles shows a significant increase in muscle size in Fc-TWEAK-treated $Smn^{2B/-}$ mice compared to untreated SMA animals (Fig. 7y–z).

While MuRF-1 and atrogin-1 are well described atrophy markers [57], whose expression has previously been well characterized in skeletal muscle of $Smn^{-/-}$;*SMN2* and $Smn^{2B/-}$ mice at various time points during disease progression [61], there is also evidence that they can be induced by the Tweak/Fn14 signaling cascade [24]. We therefore investigated their levels in quadriceps and triceps of P7 $Fn14^{-/-}$ mice (Supplementary Fig. 5) and find that while *atrogin-1* levels are unchanged compared to WT animals (Supplementary Fig. 5a), *MuRF-1* levels are significantly downregulated in both muscles of $Fn14^{-/-}$ mice, consistent with the previously reported positive correlation between Tweak/Fn14 activity and MuRF-1 expression (Supplementary Fig. 5b) [24]. These results suggest that the reduced levels of *MuRF-1* observed in skeletal muscle of Fc-TWEAK-treated SMA mice are most likely linked to improved muscle health. Furthermore, the differential effect of Fc-TWEAK on the expression of *MuRF-1* and *atrogin-1* in $Smn^{-/-}$;*SMN2* and $Smn^{2B/-}$ is most probably due to the previously reported distinct regulatory processes that contribute to muscle atrophy in both models [61].

Taken together, our results suggests that promoting Tweak activity in SMA mice has the potential to improve weight, survival and muscle pathology, suggesting that restoring the Tweak and Fn14 signaling in SMA muscle may lead to sustainable therapeutic benefits.

Discussion

Motor neuron death and muscle pathology bidirectionally impact on each other in SMA. Indeed, while loss of motor neurons significantly contributes to muscle atrophy, there is also evidence for muscle-intrinsic abnormalities in SMA skeletal muscle, which could be directly or indirectly caused by SMN deficiency [5, 6, 62–64]. In this study, we attempted to address the underlying mechanisms of muscle-intrinsic abnormalities leading to muscle pathology in SMA by investigating the role of TWEAK and Fn14 in muscle atrophy in SMA. To the best of our knowledge, this is the first study to evaluate the TWEAK and Fn14 pathway in SMA and in early stages of muscle development.

Notably, we showed decreased expression of *Tweak* and *Fn14* in skeletal muscle of two distinct SMA mouse models during disease progression, which is contrary to previous reports of increased TWEAK/Fn14 activity in experimental models of atrophy in adult muscle [52, 65, 66], suggesting that TWEAK and Fn14 may have distinct roles in skeletal muscle during development and adulthood. Indeed, *Tweak* mRNA expression is significantly lower in skeletal muscle of 30-day-old WT mice compared to 90-day-old animals, suggesting an age-dependent regulation [16]. Moreover, we observed that the dysregulation of TWEAK, Fn14 and the previously proposed metabolic effectors in skeletal muscle of pre-weaned mice appears to be influenced by intrinsic muscle impairments and not denervation, which is in contrast to what has been previously reported in experimental models of adult muscle denervation [15, 16], further suggesting distinct developmental roles for Tweak and Fn14 in skeletal muscle. Given that muscles from younger mice are more resistant to surgically-induced denervation than those from older mice [67], TWEAK and Fn14 may contribute to this age-dependent differential vulnerability of muscle to pathological insults. Thus, the role of TWEAK/Fn14 signaling in muscle pathology may be more nuanced and be influenced by a combination of factors such as absolute levels, downstream signaling cascades activated (e.g. canonical vs noncanonical NF-κB signaling pathways), developmental stage of the muscle, state of muscle atrophy (e.g, chronic vs acute) and primary origin of muscle pathology (e.g. denervation vs intrinsic insult) [11, 12].

Another key observation from our study is a potential interaction and/or overlap between Tweak, Fn14 and Smn and their downstream signaling cascades in muscle. It has previously been demonstrated that once Tweak binds to Fn14, the complex will activate several NF-κB molecular effectors, including TRAF6 and IKK [68]. Interestingly, SMN has been reported to prevent the activation of TRAF6 and IKK, thereby negatively regulating the muscle atrophy-inducing canonical NF-κB pathway [69]. These studies thus suggest converging roles for TWEAK, Fn14 and Smn in muscle, which is further supported by our findings. Indeed, we found that independent *Tweak*, *Fn14* and *Smn* depletion had an impact on each other's expression in differentiated C2C12 cells and murine muscle. Furthermore, there was an overlap of dysregulated myogenesis, myopathy and glucose metabolism genes in SMA, $Fn14^{-/-}$ and $Tweak^{-/-}$ mice. Of note, the aberrantly regulated genes in young $Tweak^{-/-}$ and $Fn14^{-/-}$ mice did not perfectly overlap, supporting previous reports of Tweak-independent roles of Fn14 during myogenesis [70]. Thus, these results suggest that aberrant expression of TWEAK and Fn14 in SMA muscle may be a consequence of combined events resulting from muscle atrophy and reduced SMN expression. However, Smn depletion most likely needs to reach pathological levels as we did not observe obvious changes in the Tweak/Fn14 signaling pathway in skeletal muscle of non-SMA hypomorphic $Smn^{2B/2B}$ and $Smn^{+/-}$ mice. Performing genome-wide RNA sequencing studies could also help elucidate the extent of shared genes and pathways regulated by TWEAK, Fn14 and SMN. Indeed, while we have focused on a subset of previously reported and proposed metabolic effectors and the NF-κB pathways, other canonical pathways such as MAPK signaling, known to have functional interactions with Tweak, Fn14 and Smn, may also display converging roles in muscle health [71, 72].

In addition, our results in developing mice do support the previously reported negative regulation of the metabolic factors Pgc-1α, Mef2d, Glut-4, Klf15 and HKII in adult muscle [18]. Further analyses of a subset of specific glucose metabolism genes showed that about 20% of these genes were dysregulated in the same direction in $Fn14^{-/-}$, $Tweak^{-/-}$ and SMA mice. Our KEGG analysis of these shared dysregulated metabolic genes further support the potential relationships and roles of TWEAK, Fn14 and SMN involved in the regulation of glucose metabolism. Indeed, the AMPK signaling pathway, found to be aberrantly regulated in $Fn14^{-/-}$, $Tweak^{-/-}$ and SMA, is as a master regulator of skeletal muscle function and metabolism [73]. Interestingly, a previous study in *SMNΔ7* SMA mice further showed that chronic treatment with the AMPK agonist AICAR prevented skeletal muscle pathology [74]. In addition, AMPK directly phosphorylates PGC-1α [75], which is also dysregulated in *Smn*-, *Tweak*- and *Fn14*-depleted models [66, 76]. We also found that glycolysis and pyruvate metabolic pathways, which culminate in the generation of ATP, are also dysregulated in SMA, $Fn14^{-/-}$ and $Tweak^{-/-}$ mice. Interestingly, siRNA-mediated *Smn* knockdown in NSC-34 cells showed a significant decrease in ATP production [77]. ATP was also decreased in $Smn^{-/-}$;*SMN2* mice and in Smn morphant zebrafish [78]. These results could explain mitochondrial dysfunction in SMA patients [5]. Thus, our study strengthens the notion of metabolic dysfunctions contributing to SMA muscle pathology and suggests a potential mechanistic link with the TWEAK/Fn14 pathway.

However, it is important to note that although our findings support the idea that the aberrant expression of *Pgc-1α*, *Mef2d*, *Glut-4*, *Klf15* and *HKII* is due to the dysregulated expression of *Tweak* and *Fn14* in SMA muscle, further mechanistic insights are required to fully understand the extent of the transcriptional regulation of these key metabolic effectors by TWEAK/Fn14 signaling in developing post-natal muscle. Indeed, their differential dysregulations in $Smn^{-/-}$;*SMN2*, $Smn^{2B/-}$, $Tweak^{-/-}$ and $Fn14^{-/-}$ muscle as well as the varying impact that Fc-Tweak injections had on their expression levels suggest that additional regulatory mechanisms may be contributing to our observations.

Our findings also confirm that not all skeletal muscles are equally affected in SMA. Indeed, we observed that the SMA skeletal muscle atrophy marker *parvalbumin* was significantly decreased from an earlier time point in the vulnerable triceps and gastrocnemius muscles than in the more resistant TA and quadriceps muscles. Notably, we also found that 20% more myogenesis- and myopathy-related genes were dysregulated in the more vulnerable triceps muscles of $Smn^{-/-}$;*SMN2* mice compared to the resistant quadriceps muscles. Conversely, the number of glucose metabolism genes dysregulated in SMA triceps and quadriceps muscles was not significantly different. Previous studies have reported that muscle vulnerability is more closely associated with NMJ denervation than with location or fiber-type composition [35]. Our results further suggest that denervation events in vulnerable SMA muscles have a more prominent effect on myogenesis and myopathy than on glucose metabolism.

Finally, modulating Tweak activity via Fc-TWEAK in two SMA mouse models led to interesting observations. Firstly, Fc-TWEAK administration specifically increased life span in the milder $Smn^{2B/-}$ mouse model, while it did not impact disease progression in the severe $Smn^{-/-}$;*SMN2* mice. This is consistent with previous studies, including ours, demonstrating that the

Smn$^{2B/-}$ mice are more responsive to non-SMN interventions, perhaps due to their longer asymptomatic, and therefore adaptable, period [41, 58–60, 79]. At a molecular level, we found that Fc-TWEAK differentially impacted the expression of the *Tweak*, *Fn14* and the previously proposed metabolic effectors in SMA mice and healthy littermates in a time-dependent manner, perhaps reflecting disease state-dependent regulatory mechanisms of the pathway. Importantly, the expression of *Mef2d*, *HKII* and *Klf15* was significantly downregulated in Fc-TWEAK-treated SMA mice, supporting an increased activity of Tweak in the mice and a subsequent restoration towards normal levels of aberrantly expressed proposed Tweak/Fn14 effectors. As mentioned above, the timing between Fc-TWEAK administration and tissue collection may have limited our analysis of the effect of Fc-TWEAK on the Tweak/Fn14 signaling cascade. Furthermore, our focus on the specific subset of previously reported proposed metabolic effectors (*Pgc-1α*, *Mef2d*, *Glut-4*, *Klf15* and *HKII*) probably also resulted in us not having a complete picture of the molecular impacts of Fc-TWEAK. Indeed, Fc-TWEAK may have affected the expression of the shared aberrantly expressed genes identified with the myogenesis, myopathy, and glucose metabolism PCR arrays such as *Pax7* and *Titin* as well as the abovementioned pathways (e.g. MAPK and AMPK). Nevertheless, administration of Fc-TWEAK did improve muscle pathology in SMA mice as demonstrated by the partial restoration of molecular markers of muscle health and myofiber size. These results support a role for the TWEAK/Fn14 pathway in maintaining skeletal muscle health and homeostasis [12]. However, it is important to note that the TWEAK/Fn14 pathway is involved in many other tissues and pathologies such as tumor development and metastasis, heart-related diseases [80], kidney injury, cerebral ischemia [81, 82] and autoimmune diseases [83, 84], which could have influenced the overall impact of systemically administered Fc-TWEAK on muscle health and disease progression in SMA mice.

Conclusion

In summary, our results suggest a potential role and contribution of the TWEAK/Fn14 pathway to myopathy and glucose metabolism perturbations in SMA muscle. Furthermore, our study, combined with previous work in adult models [11, 12], proposes that dysregulation of the TWEAK/Fn14 signaling in muscle appears to be dependent on the origin of the muscle pathology (e.g. denervation vs intrinsic) and developmental stage of skeletal muscle (e.g. newborn, juvenile, adult, aged), further highlighting the differential and conflicting activities of the pathway. Future investigations should therefore be aimed at both furthering our understanding of the relevance of the Tweak/Fn14 pathway in SMA muscle and defining its role in general in maintaining muscle homeostasis throughout the life course.

Abbreviations

ALS: Amyotrophic lateral sclerosis; ANOVA: Analysis of variance; cDNA: Complementary deoxyribonucleic acid; DEGs: Differently expressed genes; DMEM: Dulbecco's Modified Eagle's Media; FBS: Fetal bovine serum; FDR: False discovery rate; GO: Gene ontology; H&E: Hematoxylin and eosin; KEGG: Kyoto Encyclopedia of Genes and Genomes; mRNA: Messenger RNA; NF-κB: Nuclear factor kappa-light-chain-enhancer of activated B cells; NMJ: Neuromuscular junction; P: Post-natal day; *p*: Probability value; PBS: Phosphate-buffered saline; PCR: Polymerase chain reaction; PFA: Paraformaldehyde; qPCR: Quantitative polymerase chain reaction; RIPA: Radioimmunoprecipitation; RNA: Ribonucleic acid; RNAi: RNA interference; RT-qPCR: Reverse transcriptase-quantitative PCR; SEM: Standard error of the mean; siRNA: Small interfering RNA; SMA: Spinal muscular atrophy; STRING: Search Tool for the Retrieval of Interacting Genes/Proteins; TA: *Tibialis anterior*; WT: Wild-type.

Supplementary Information

The online version contains supplementary material available at https://doi.org/10.1186/s13395-022-00301-z.

Additional file 1: Supplementary Figure 1. No overt dysregulation of Tweak and Fn14 in skeletal muscle of non-SMA hypomorphic Smn-depleted mice. qPCR analysis of *Tweak* (a), *Fn14* (b), *Pgc-1α* (c), *Mef2d* (d), *Glut*-4 (e), *HKII* (f) and *Klf15* (g) in triceps from post-natal day (P) 7 wild-type (WT), *Smn*$^{2B/2B}$ and *Smn*$^{+/-}$ mice. Normalized relative expressions are compared to WT. Data are mean ± SEM, $n = 4$-5 animals per experimental group, one-way ANOVA, Tukey's multiple comparison test, * $p < 0.05$, ns = not significant. **Supplementary Figure 2.** Tweak and Fn14 are not dysregulated in denervated (nerve cut) muscles of pre-weaned mice. A sciatic nerve cut was performed on post-natal day (P) 7 WT FVB/N mice and both ipsilateral (nerve cut) and contralateral (control) TA muscles were harvested at P14. qPCR analysis of *Tweak*, *Fn14*, *Pgc-1α*, *Mef2d*, *Glut-4*, *HKII* and *Klf15* in control and nerve cut TA muscles. Normalized relative expressions for each gene are compared to control muscle. Data are mean ± SEM, $n = 7$-11 animals per experimental group, two-way ANOVA, uncorrected Fisher's LSD, ns = not significant. **Supplementary Figure 3.** Effect of varying Fc-TWEAK doses on disease progression in *Smn*$^{-/-}$*;SMN2* SMA mice. *Smn*$^{-/-}$*;SMN2* mice received daily subcutaneous injections of increasing doses of Fc-TWEAK (7.9, 15., 23.7 and 31.6 µg), starting at birth. a. Daily weights of untreated *Smn*$^{-/-}$*;SMN2* SMA mice and *Smn*$^{-/-}$*;SMN2* mice that received daily subcutaneous injections (starting at P0) of Fc-TWEAK (7.9, 15.8, 23.7 and 31.6 µg). Data are mean ± SEM, $n =$ 5-10 animals per experimental group, two-way ANOVA, Sidak's multiple comparison test. b. Survival curves of untreated *Smn*$^{-/-}$*;SMN2* SMA mice and *Smn*$^{-/-}$*;SMN2* mice that received daily subcutaneous injections (starting at P0) of Fc-TWEAK (7.9, 15.8, 23.7 and 31.6 µg). Data are presented as Kaplan-Meier survival curves, $n = 5$-10 animals per experimental group, Log-rank (Mantel-Cox). **Supplementary Figure 4.** Differential effect of Fc-TWEAK in skeletal muscle of wild type (WT) and *Smn*$^{2B/-}$ mice. WT and *Smn*$^{2B/-}$ SMA mice and received subcutaneous injections of Fc-TWEAK (15.8 µg) every 4 days (from post-natal day (P) 0 to P16) and skeletal muscles were harvested 3 hours post-injections. a-g. qPCR analysis of *Fn14* (**a**), *Tweak* (**b**), *Pgc-1α* (**c**), *Mef2d* (**d**), *Glut-4* (**e**), *HKII* (**f**) and *Klf15* (**g**) in triceps of untreated and Fc-TWEAK-treated *Smn*$^{2B/-}$ mice. Normalized relative expressions for Fc-TWEAK-treated WT mice are compared to untreated WT mice and normalized relative expressions for Fc-TWEAK-treated *Smn*$^{2B/-}$ mice are compared to untreated *Smn*$^{2B/-}$ mice. Data are mean ± SEM, n = 3-5 animals per experimental group, two-way ANOVA, uncorrected Fisher's LSD, * $p < 0.05$, ** $p < 0.01$, *** $p < 0.001$, **** $p < 0.0001$, ns = not significant. **h**. Quantification of NF-κB2 p100 protein levels normalized to total protein in the quadriceps of late-symptomatic (P18) *Smn*$^{2B/-}$ mice and age-matched WT animals. Images are representative immunoblots. Data are mean ± SEM, $n = 3$-5 animals per experimental group**,** unpaired *t* test, $p = 0.0005$ (WT), $p = 0.0494$. **Supplementary Figure 5.** Decreased

MuRF-1 expression in skeletal muscle of P7 *Fn14*$^{-/-}$ mice. qPCR analysis of *Atrogin-1* (**a**) and *MuRF-1* (**b**) in quadriceps and triceps from post-natal day (P) 7 wild type (WT) and *Fn14*$^{-/-}$ mice. Normalized relative expressions are compared to WT. Data are mean ± SEM, $n = 4$ animals per experimental group, unpaired *t* test, $p = 0.0164$ (*MuRF-1* quadriceps), $p = 0.0283$ (*MuRF-1* triceps), ns = not significant.

Additional file 2: Supplementary Table 1. Mouse primers used for quantitative real-time PCR.

Additional file 3: Supplementary file 1. Myopathy and myogenesis gene expression changes in triceps and quadriceps of post-natal day 7 *Smn*$^{-/-}$*;SMN2* (SMA), *Tweak*$^{-/-}$ (Tweak KO) and *Fn14*$^{-/-}$; (Fn14 KO) compared to age- and genetic strain-matched wild type animals.

Additional file 4: Supplementary file 2. Glucose metabolism gene expression changes in triceps and quadriceps of post-natal day 7 *Smn*$^{-/-}$*;SMN2* (SMA), *Tweak*$^{-/-}$ (Tweak KO) and *Fn14*$^{-/-}$; (Fn14 KO) compared to age- and genetic strain-matched wild type animals.

Acknowledgements
We would like to thank the staff at the BMS facility at the University of Oxford and the BSU facility at Keele University.

Authors' contributions
Conceptualization, MB; methodology, KEM, ERS, and MB; validation, KEM and M; formal analysis, KEM, RS, EM, EM, SK, and MB; investigations, KEM, ERS, EM, MDA, B, SK, IT, IB, GH, NA, and MB; writing—original draft preparation, KEM and MB; writing — review and editing, KEM, ERS, EM, EM, DA, BE, SK, IT, IB, GH, NA, PC, KED, RK, MJAW, and MB; visualization, KEM, ERS, EM, and MB; supervision, PC, KED, RK, MJAW, and MB; project administration, MB; funding acquisition, RK, MJAW, and MB. The authors read and approved the final manuscript.

Funding
KEM was funded by the MDUK and SMA Trust (now SMA UK). MB was funded by the SMA Trust (now SMA UK) and Muscular Dystrophy Ireland/MRCG-HRB (MRCG-2016-21). SK was supported by an ERASMUS grant. PC received financial support from the Deutsche Muskelstiftung. RK was funded by the Canadian Institutes of Health Research and Muscular Dystrophy Association (USA). ERS is funded by a MDUK studentship (18GRO-PS48-0114). EM is supported by an Academy of Medical Sciences grant (SBF006/1162)

Availability of data and materials
All data generated or analyzed during this study are included in this published article or in the supplementary information.

Declarations

Ethics approval and consent to participate
Experimental procedures with live animals were authorized and approved by the University of Oxford ethics committee and UK Home Office (current project license PDFEDC6F0, previous project license 30/2907) in accordance with the Animals (Scientific Procedures) Act 1986, the Keele University Animal Welfare Ethical Review Body and UK Home Office (Project License P99AB3B95) in accordance with the Animals (Scientific Procedures) Act 1986, the University of Ottawa Animal Care Committee according to procedures authorized by the Canadian Council on Animal Care and the German Animal Welfare law and approved by the Lower Saxony State Office for Consumer Protection and Food Safety (LAVES, reference numbers 15/1774 and 19/3309).

Consent for publication
Not applicable.

Competing interests
The authors declare that they have no competing interests.

Author details
[1]Department of Physiology, Anatomy and Genetics, University of Oxford, Oxford, UK. [2]Gene Therapy Center, UMass Medical School, Worcester, USA. [3]School of Medicine, Keele University, Staffordshire, UK. [4]Regenerative Medicine Program and Department of Cellular and Molecular Medicine, Ottawa Hospital Research Institute and University of Ottawa, Ottawa, Canada. [5]Department of Pharmacology, University of Oxford, Oxford, UK. [6]Center for Systems Neuroscience and Institute of Neuroanatomy and Cell Biology, Hannover Medical School, Hannover, Germany. [7]SMATHERIA — Non-Profit Biomedical Research Institute, Hannover, Germany. [8]Department of Paediatrics, University of Oxford, Oxford, UK. [9]Wolfson Centre for Inherited Neuromuscular Disease, RJAH Orthopaedic Hospital, Oswestry, UK.

Received: 13 September 2021 Accepted: 10 July 2022
Published online: 28 July 2022

References

1. Miniño AM, Xu J, Kochanek KD. National Vital Statistics Reports, Volume 59, Number 2, (December 9, 2010); 2008.
2. Lefebvre S, Bürglen L, Reboullet S, Clermont O, Burlet P, Viollet L, et al. Identification and characterization of a spinal muscular atrophy-determining gene. Cell. 1995;80:155–65.
3. Crawford TO, Pardo CA. The neurobiology of childhood spinal muscular atrophy. Neurobiol Dis. 1996;3:97–110.
4. Swoboda KJ, Prior TW, Scott CB, McNaught TP, Wride MC, Reyna SP, et al. Natural History of denervation in SMA: relation to age, SMN2 copy number, and function. Ann Neurol. 2005;57:704–12.
5. Ripolone M, Ronchi D, Violano R, Vallejo D, Fagiolari G, Barca E, et al. Impaired muscle mitochondrial biogenesis and myogenesis in spinal muscular atrophy. JAMA Neurol. 2015;72:666–75 NIH Public Access.
6. Shafey D, Côté PD, Kothary R. Hypomorphic Smn knockdown C2C12 myoblasts reveal intrinsic defects in myoblast fusion and myotube morphology. Exp Cell Res. 2005;311:49–61 Academic Press.
7. Stump CS, Henriksen EJ, Wei Y, Sowers JR. The metabolic syndrome: role of skeletal muscle metabolism. Ann Med. 2006;38:389–402.
8. Deguise M-O, Chehade L, Kothary R. Metabolic dysfunction in spinal muscular atrophy. Int J Mol Sci. 2021;22:5913.
9. Boyer JG, Ferrier A, Kothary R. More than a bystander: the contributions of intrinsic skeletal muscle defects in motor neuron diseases. Front Physiol. 2013;4:356 Frontiers Media SA.
10. Carmona Arana JA, Seher A, Neumann M, Lang I, Siegmund D, Wajant H. TNF receptor-associated factor 1 is a major target of soluble TWEAK. Front Immunol. 2014;5:63 Frontiers Media SA.
11. Enwere EK, Lacasse EC, Adam NJ, Korneluk RG. Role of the TWEAK-Fn14-cIAP1-NF-κB signaling axis in the regulation of myogenesis and muscle homeostasis. Front Immunol. 2014;5:34.
12. Pascoe AL, Johnston AJ, Murphy RM. Controversies in TWEAK-Fn14 signaling in skeletal muscle atrophy and regeneration. Cell Mol Life Sci. 2020;77(17):3369–81. https://doi.org/10.1007/s00018-020-03495-x.
13. Merritt EK, Thalacker-Mercer A, Cross JM, Windham ST, Thomas SJ, Bamman MM. Increased expression of atrogenes and TWEAK family members after severe burn injury in nonburned human skeletal muscle. J Burn Care Res Off Publ Am Burn Assoc. 2013;34:e297–304.
14. Meighan-Mantha RL, Hsu DK, Guo Y, Brown SA, Feng SL, Peifley KA, et al. The mitogen-inducible Fn14 gene encodes a type I transmembrane protein that modulates fibroblast adhesion and migration. J Biol Chem. 1999;274:33166–76.
15. Mittal A, Bhatnagar S, Kumar A, Lach-Trifilieff E, Wauters S, Li H, et al. The TWEAK-Fn14 system is a critical regulator of denervation-induced skeletal muscle atrophy in mice. J Cell Biol. 2010;188:833–49.
16. Bowerman M, Salsac C, Coque E, Eiselt É, Deschaumes RG, Brodovitch A, et al. Tweak regulates astrogliosis, microgliosis and skeletal muscle atrophy in a mouse model of amyotrophic lateral sclerosis. Hum Mol Genet. 2015;24:3440–56.
17. Arany Z. PGC-1 coactivators and skeletal muscle adaptations in health and disease. Curr Opin Genet Dev. 2008;18:426–34.
18. Sato S, Ogura Y, Tajrishi MM, Kumar A. Elevated levels of TWEAK in skeletal muscle promote visceral obesity, insulin resistance, and metabolic dysfunction. FASEB J Off Publ Fed Am Soc Exp Biol. 2015;29:988–1002.
19. Roberts DJ, Miyamoto S. Hexokinase II integrates energy metabolism and cellular protection: Akting on mitochondria and TORCing to autophagy. Cell Death Differ. 2015;22:248–57.

20. Fan L, Hsieh PN, Sweet DR, Jain MK. Krüppel-like factor 15: regulator of BCAA metabolism and circadian protein rhythmicity. Pharmacol Res. 2018;130:123–6.
21. Wood MJA, Talbot K, Bowerman M. Spinal muscular atrophy: antisense oligonucleotide therapy opens the door to an integrated therapeutic landscape. Hum Mol Genet. 2017;26:R151–9.
22. Hsieh-Li HM, Chang JG, Jong YJ, Wu MH, Wang NM, Tsai CH, et al. A mouse model for spinal muscular atrophy. Nat Genet. 2000;24:66–70.
23. Bowerman M, Murray LM, Beauvais A, Pinheiro B, Kothary R. A critical smn threshold in mice dictates onset of an intermediate spinal muscular atrophy phenotype associated with a distinct neuromuscular junction pathology. Neuromuscul Disord NMD. 2012;22:263–76.
24. Sato S, Ogura Y, Kumar A. TWEAK/Fn14 signaling axis mediates skeletal muscle atrophy and metabolic dysfunction. Front Immunol. 2014;5:18.
25. Eshraghi M, McFall E, Gibeault S, Kothary R. Effect of genetic background on the phenotype of the Smn2B/- mouse model of spinal muscular atrophy. Hum Mol Genet. 2016;25:4494–506.
26. Campbell S, Burkly LC, Gao H-X, Berman JW, Su L, Browning B, et al. Proinflammatory effects of TWEAK/Fn14 interactions in glomerular mesangial cells. J Immunol Baltim Md. 1950;2006(176):1889–98.
27. Jakubowski A, Ambrose C, Parr M, Lincecum JM, Wang MZ, Zheng TS, et al. TWEAK induces liver progenitor cell proliferation. J Clin Invest. 2005;115:2330–40.
28. Riessland M, Ackermann B, Förster A, Jakubik M, Hauke J, Garbes L, et al. SAHA ameliorates the SMA phenotype in two mouse models for spinal muscular atrophy. Hum Mol Genet. 2010;19:1492–506.
29. Schindelin J, Arganda-Carreras I, Frise E, Kaynig V, Longair M, Pietzsch T, et al. Fiji: an open-source platform for biological-image analysis. Nat Methods. 2012;9:676–82 Nature Publishing Group.
30. Yaffe D, Saxel O. Serial passaging and differentiation of myogenic cells isolated from dystrophic mouse muscle. Nature. 1977;270:725–7 Nature Publishing Group.
31. Cashman NR, Durham HD, Blusztajn JK, Oda K, Tabira T, Shaw IT, et al. Neuroblastoma × spinal cord (NSC) hybrid cell lines resemble developing motor neurons. Dev Dyn. 1992;194:209–21.
32. Pfaffl MW. A new mathematical model for relative quantification in real-time RT-PCR. Nucleic Acids Res. 2001;29:45e–45 Oxford University Press (OUP).
33. Radonić A, Thulke S, Mackay IM, Landt O, Siegert W, Nitsche A. Guideline to reference gene selection for quantitative real-time PCR. Biochem Biophys Res Commun. 2004;313:856–62.
34. Szklarczyk D, Morris JH, Cook H, Kuhn M, Wyder S, Simonovic M, et al. The STRING database in 2017: quality-controlled protein–protein association networks, made broadly accessible. Nucleic Acids Res. 2017;45:D362–8.
35. Ling KKY, Gibbs RM, Feng Z, Ko C-PC-P. Severe neuromuscular denervation of clinically relevant muscles in a mouse model of spinal muscular atrophy. Hum Mol Genet. 2012;21:185–95.
36. Boyer JG, Murray LM, Scott K, De Repentigny Y, Renaud J-M, Kothary R. Early onset muscle weakness and disruption of muscle proteins in mouse models of spinal muscular atrophy. Skelet Muscle. 2013;3:24.
37. Boyer JG, Deguise M-O, Murray LM, Yazdani A, De Repentigny Y, Boudreau-Larivière C, et al. Myogenic program dysregulation is contributory to disease pathogenesis in spinal muscular atrophy. Hum Mol Genet. 2014;23:4249–59.
38. Olive M, Ferrer I. Parvalbumin immunohistochemistry in denervated skeletal muscle. Neuropathol Appl Neurobiol. 1994;20:495–500.
39. Müntener M, Berchtold MW, Heizmann CW. Parvalbumin in cross-reinnervated and denervated muscles. Muscle Nerve. 1985;8:132–7.
40. Mutsaers CA, Wishart TM, Lamont DJ, Riessland M, Schreml J, Comley LH, et al. Reversible molecular pathology of skeletal muscle in spinal muscular atrophy. Hum Mol Genet. 2011;20:4334–44.
41. Walter LM, Deguise M-O, Meijboom KE, Betts CA, Ahlskog N, van Westering TLE, et al. Interventions targeting glucocorticoid-Krüppel-like factor 15-branched-chain amino acid signaling improve disease phenotypes in spinal muscular atrophy mice. EBioMedicine. 2018;31:226–42.
42. Li H, Mittal A, Paul PK, Kumar M, Srivastava DS, Tyagi SC, et al. Tumor necrosis factor-related weak inducer of apoptosis augments matrix metalloproteinase 9 (MMP-9) production in skeletal muscle through the activation of nuclear factor-κB-inducing kinase and p38 mitogen-activated protein kinase. J Biol Chem. 2009;284:4439–50.
43. Varfolomeev E, Goncharov T, Maecker H, Zobel K, Kömüves LG, Deshayes K, et al. Cellular inhibitors of apoptosis are global regulators of NF-κB and MAPK activation by members of the TNF family of receptors. Sci Signal. 2012;5:ra22.
44. Li Y, Kang J, Friedman J, Tarassishin L, Ye J, Kovalenko A, et al. Identification of a cell protein (FIP-3) as a modulator of NF-B activity and as a target of an adenovirus inhibitor of tumor necrosis factor -induced apoptosis. Proc Natl Acad Sci. 1999;96:1042–7 National Academy of Sciences.
45. Bowerman M, Michalski J-P, Beauvais A, Murray LM, DeRepentigny Y, Kothary R. Defects in pancreatic development and glucose metabolism in SMN-depleted mice independent of canonical spinal muscular atrophy neuromuscular pathology. Hum Mol Genet. 2014;23:3432–44.
46. Magill CK, Tong A, Kawamura D, Hayashi A, Hunter DA, Parsadanian A, et al. Reinnervation of the tibialis anterior following sciatic nerve crush injury: a confocal microscopic study in transgenic mice. Exp Neurol. 2007;207:64–74 NIH Public Access.
47. Yan Z, Choi S, Liu X, Zhang M, Schageman JJ, Lee SY, et al. Highly coordinated gene regulation in mouse skeletal muscle regeneration. J Biol Chem. 2003;278:8826–36 American Society for Biochemistry and Molecular Biology.
48. Mittal A, Bhatnagar S, Kumar A, Paul PK, Kuang S, Kumar A. Genetic ablation of TWEAK augments regeneration and post-injury growth of skeletal muscle in mice. Am J Pathol. 2010;177:1732–42.
49. Kariya S, Obis T, Garone C, Akay T, Sera F, Iwata S, et al. Requirement of enhanced survival motoneuron protein imposed during neuromuscular junction maturation. J Clin Invest. 2014;124:785–800.
50. Garry GA, Antony ML, Garry DJ. Cardiotoxin induced injury and skeletal muscle regeneration. In: Kyba M, editor. Skelet Muscle Regen Mouse Methods Protoc. New York: Springer; 2016. p. 61–71. [cited 2020 May 28]. https://doi.org/10.1007/978-1-4939-3810-0_6.
51. Girgenrath M, Weng S, Kostek CA, Browning B, Wang M, Brown SAN, et al. TWEAK, via its receptor Fn14, is a novel regulator of mesenchymal progenitor cells and skeletal muscle regeneration. EMBO J. 2006;25:5826–39.
52. Shuichi Sato YOMMTAK, Sato S, Ogura Y, Tajrishi MM, Kumar A. Elevated levels of TWEAK in skeletal muscle promote visceral obesity, insulin resistance, and metabolic dysfunction. FASEB J Off Publ Fed Am Soc Exp Biol. The Federation of American Societies for. Exp Biol. 2015;29:988–1002.
53. Yin H, Price F, Rudnicki MA. Satellite cells and the muscle stem cell niche. Physiol Rev. 2013;93:23–67.
54. von Maltzahn J, Jones AE, Parks RJ, Rudnicki MA. Pax7 is critical for the normal function of satellite cells in adult skeletal muscle. Proc Natl Acad Sci U S A. 2013;110:16474–9 National Academy of Sciences.
55. Savarese M, Sarparanta J, Vihola A, Udd B, Hackman P. Increasing role of titin mutations in neuromuscular disorders. J Neuromuscul Dis. 2016;3:293–308 IOS Press.
56. Bowerman M, Swoboda KJ, Michalski J-P, Wang G-S, Reeks C, Beauvais A, et al. Glucose metabolism and pancreatic defects in spinal muscular atrophy. Ann Neurol. 2012;72:256–68.
57. Bodine SC, Latres E, Baumhueter S, Lai VK, Nunez L, Clarke BA, et al. Identification of ubiquitin ligases required for skeletal muscle atrophy. Science. 2001;294:1704–8 American Association for the Advancement of Science.
58. Bowerman M, Beauvais A, Anderson CL, Kothary R. Rho-kinase inactivation prolongs survival of an intermediate SMA mouse model. Hum Mol Genet. 2010;19:1468–78.
59. Kaifer KA, Villalón E, Osman EY, Glascock JJ, Arnold LL, Cornelison DDW, et al. Plastin-3 extends survival and reduces severity in mouse models of spinal muscular atrophy. JCI Insight. 2017;2:e89970.
60. Osman EY, Rietz A, Kline RA, Cherry JJ, Hodgetts KJ, Lorson CL, et al. Intraperitoneal delivery of a novel drug-like compound improves disease severity in severe and intermediate mouse models of spinal muscular atrophy. Sci Rep. 2019;9:1633.
61. Deguise M-O, Boyer JG, McFall ER, Yazdani A, De Repentigny Y, Kothary R. Differential induction of muscle atrophy pathways in two mouse models of spinal muscular atrophy. Sci Rep. 2016;6:28846.
62. Martínez-Hernández R, Soler-Botija C, Also E, Alias L, Caselles L, Gich I, et al. The developmental pattern of myotubes in spinal muscular atrophy indicates prenatal delay of muscle maturation. J Neuropathol Exp Neurol. 2009;68:474–81 Oxford University Press.
63. Martínez-Hernández R, Bernal S, Alias L, Tizzano EF. Abnormalities in early markers of muscle involvement support a delay in myogenesis in spinal

muscular atrophy. J Neuropathol Exp Neurol. 2014;73:559–67 Oxford University Press.
64. Rajendra TK, Gonsalvez GB, Walker MP, Shpargel KB, Salz HK, Matera AG. A Drosophila melanogaster model of spinal muscular atrophy reveals a function for SMN in striated muscle. J Cell Biol. 2007;176:831–41.
65. Liu H, Peng H, Xiang H, Guo L, Chen R, Zhao S, et al. TWEAK/Fn14 promotes oxidative stress through AMPK/PGC-1α/MnSOD signaling pathway in endothelial cells. Mol Med Rep. 2017;17:1998–2004 Spandidos Publications.
66. Hindi SM, Mishra V, Bhatnagar S, Tajrishi MM, Ogura Y, Yan Z, et al. Regulatory circuitry of TWEAK-Fn14 system and PGC-1α in skeletal muscle atrophy program. FASEB J Off Publ Fed Am Soc Exp Biol. 2014;28:1398–411.
67. Murray LM, Comley LH, Gillingwater TH, Parson SH. The response of neuromuscular junctions to injury is developmentally regulated. FASEB J. 2011;25:1306–13.
68. Kumar A, Bhatnagar S, Paul PK. TWEAK and TRAF6 regulate skeletal muscle atrophy. Curr Opin Clin Nutr Metab Care. 2012;15:233–9 NIH Public Access.
69. Kim EK, Choi E-J. SMN1 functions as a novel inhibitor for TRAF6-mediated NF-κB signaling. Biochim Biophys Acta BBA - Mol Cell Res. 2017;1864:760–70 Elsevier.
70. Dogra C, Hall SL, Wedhas N, Linkhart TA, Kumar A. Fibroblast growth factor inducible 14 (Fn14) is required for the expression of myogenic regulatory factors and differentiation of myoblasts into myotubes. Evidence for TWEAK-independent functions of Fn14 during myogenesis. J Biol Chem. 2007;282:15000–10.
71. Li H, Mittal A, Paul PK, Kumar M, Srivastava DS, Tyagi SC, et al. Tumor necrosis factor-related weak inducer of apoptosis augments matrix metalloproteinase 9 (MMP-9) production in skeletal muscle through the activation of nuclear factor-kappaB-inducing kinase and p38 mitogen-activated protein kinase: a potential role of MMP-9 in myopathy. J Biol Chem. 2009;284:4439–50.
72. Farooq F, Balabanian S, Liu X, Holcik M, MacKenzie A. p38 Mitogen-activated protein kinase stabilizes SMN mRNA through RNA binding protein HuR. Hum Mol Genet. 2009;18:4035–45.
73. Kjøbsted R, Hingst JR, Fentz J, Foretz M, Sanz M-N, Pehmøller C, et al. AMPK in skeletal muscle function and metabolism. FASEB J Off Publ Fed Am Soc Exp Biol. 2018;32:1741–77.
74. Cerveró C, Montull N, Tarabal O, Piedrafita L, Esquerda JE, Calderó J. Chronic treatment with the AMPK agonist AICAR prevents skeletal muscle pathology but fails to improve clinical outcome in a mouse model of severe spinal muscular atrophy. Neurother J Am Soc Exp Neurother. 2016;13:198–216 Springer.
75. Irrcher I, Ljubicic V, Kirwan AF, Hood DA. AMP-activated protein kinase-regulated activation of the PGC-1α promoter in skeletal muscle cells. Lucia A, editor. PLoS One. 2008;3:e3614.
76. Ng SY, Mikhail A, Ljubicic V. Mechanisms of exercise-induced survival motor neuron expression in the skeletal muscle of spinal muscular atrophy-like mice. J Physiol. 2019;597:4757–78.
77. Acsadi G, Lee I, Li X, Khaidakov M, Pecinova A, Parker GC, et al. Mitochondrial dysfunction in a neural cell model of spinal muscular atrophy. J Neurosci Res. 2009;87:2748–56.
78. Boyd PJ, Tu W-Y, Shorrock HK, Groen EJN, Carter RN, Powis RA, et al. Bioenergetic status modulates motor neuron vulnerability and pathogenesis in a zebrafish model of spinal muscular atrophy. Cox GA, editor. PLoS Genet. 2017;13:e1006744 Public Library of Science.
79. Bowerman M, Murray LM, Boyer JG, Anderson CL, Kothary R. Fasudil improves survival and promotes skeletal muscle development in a mouse model of spinal muscular atrophy. BMC Med. 2012;10:24.
80. Jain M, Jakubowski A, Cui L, Shi J, Su L, Bauer M, et al. A novel role for tumor necrosis factor-like weak inducer of apoptosis (TWEAK) in the development of cardiac dysfunction and failure. Circulation. 2009;119:2058–68.
81. Inta I, Frauenknecht K, Dörr H, Kohlhof P, Rabsilber T, Auffarth GU, et al. Induction of the cytokine TWEAK and its receptor Fn14 in ischemic stroke. J Neurol Sci. 2008;275:117–20.
82. Haile WB, Echeverry R, Wu F, Guzman J, An J, Wu J, et al. Tumor necrosis factor-like weak inducer of apoptosis and fibroblast growth factor-inducible 14 mediate cerebral ischemia-induced poly(ADP-ribose) polymerase-1 activation and neuronal death. Neuroscience. 2010;171:1256–64.
83. Yamana J, Morand EF, Manabu T, Sunahori K, Takasugi K, Makino H, et al. Inhibition of TNF-induced IL-6 by the TWEAK-Fn14 interaction in rheumatoid arthritis fibroblast like synoviocytes. Cell Immunol. 2012;272:293–8.
84. El-shehaby A, Darweesh H, El-Khatib M, Momtaz M, Marzouk S, El-Shaarawy N, et al. Correlations of urinary biomarkers, TNF-like weak inducer of apoptosis (TWEAK), osteoprotegerin (OPG), monocyte chemoattractant protein-1 (MCP-1), and IL-8 with lupus nephritis. J Clin Immunol. 2011;31:848–56.

Publisher's Note